IFN-γ drives inflammatory bowel disease pathogenesis through VE-cadherin–directed vascular barrier disruption

Victoria Langer,[1] Eugenia Vivi,[1] Daniela Regensburger,[1] Thomas H. Winkler,[2] Maximilian J. Waldner,[3] Timo Rath,[3] Benjamin Schmid,[4] Lisa Skottke,[1] Somin Lee,[5] Noo Li Jeon,[5] Thomas Wohlfahrt,[6] Viktoria Kramer,[3] Philipp Tripal,[4] Michael Schumann,[7] Stephan Kersting,[8] Claudia Handtrack,[8] Carol I. Geppert,[9] Karina Suchowski,[10] Ralf H. Adams,[11] Christoph Becker,[3] Andreas Ramming,[6] Elisabeth Naschberger,[1] Nathalie Britzen-Laurent,[1] and Michael Stürzl[1]

[1]Division of Molecular and Experimental Surgery, Translational Research Center, Department of Surgery, University Medical Center Erlangen, [2]Division of Genetics, Nikolaus-Fiebiger-Center of Molecular Medicine, [3]Department of Medicine 1, Gastroenterology, Pneumology and Endocrinology, University Medical Center Erlangen, and [4]Optical Imaging Centre, Friedrich-Alexander University Erlangen-Nürnberg, Erlangen, Germany. [5]Program for Bioengineering, School of Engineering, Seoul National University, Seoul, Republic of Korea. [6]Department of Internal Medicine 3, Rheumatology and Immunology, University Medical Center Erlangen, Friedrich-Alexander University Erlangen-Nürnberg, Erlangen, Germany. [7]Medical Clinic I, Campus Benjamin Franklin, Charité-Universitätsmedizin Berlin, Berlin, Germany. [8]Department of Surgery and [9]Institute of Pathology, University Medical Center Erlangen, Friedrich-Alexander University Erlangen-Nürnberg, Erlangen, Germany. [10]Discovery Oncology, Pharmaceutical Research and Early Development (pRED), Roche Innovation Center Munich, Penzberg, Germany. [11]Department of Tissue Morphogenesis, Max Planck Institute for Molecular Biomedicine, Münster, Germany.

Inflammatory bowel disease (IBD) is a chronic inflammatory disorder with rising incidence. Diseased tissues are heavily vascularized. Surprisingly, the pathogenic impact of the vasculature in IBD and the underlying regulatory mechanisms remain largely unknown. IFN-γ is a major cytokine in IBD pathogenesis, but in the context of the disease, it is almost exclusively its immune-modulatory and epithelial cell–directed functions that have been considered. Recent studies by our group demonstrated that IFN-γ also exerts potent effects on blood vessels. Based on these considerations, we analyzed the vessel-directed pathogenic functions of IFN-γ and found that it drives IBD pathogenesis through vascular barrier disruption. Specifically, we show that inhibition of the IFN-γ response in vessels by endothelial-specific knockout of IFN-γ receptor 2 ameliorates experimentally induced colitis in mice. IFN-γ acts pathogenic by causing a breakdown of the vascular barrier through disruption of the adherens junction protein VE-cadherin. Notably, intestinal vascular barrier dysfunction was also confirmed in human IBD patients, supporting the clinical relevance of our findings. Treatment with imatinib restored VE-cadherin/adherens junctions, inhibited vascular permeability, and significantly reduced colonic inflammation in experimental colitis. Our findings inaugurate the pathogenic impact of IFN-γ–mediated intestinal vessel activation in IBD and open new avenues for vascular-directed treatment of this disease.

Introduction

Inflammatory bowel disease (IBD), including the 2 major forms Crohn's disease and ulcerative colitis, represents chronic inflammatory disorders of the small and large intestine (1). Classically considered as a disease of Westernized countries, the incidence of IBD has started to rise worldwide at the turn of the 21st century (2).

IBD pathogenesis is closely associated with a loss of intestinal epithelial barrier functions that can lead to excessive bacterial translocation, which might represent an initiating or early event in the disease. The characteristic chronically relapsing intestinal inflammation of IBD is thought to result from an exaggerated immune response to the commensal microbiota. Cytokines, such as IFN-γ, are considered major drivers of this excessive immune response, leading to massive leukocyte infiltration and mucosal damage (3–5).

Only recently, it has been recognized that the intestinal vascular endothelium represents a second important barrier in the gut (6). Situated between the bloodstream and the epithelial barrier, the intestinal vascular endothelium regulates blood supply, nutrient transport, tissue fluid homeostasis, and immune cell transmigration, while being nonpermissive to bacterial penetration (6–9). During IBD, inflammation has been shown to activate angiogenesis (7, 10). In accord with this, increased levels of angiogenic growth factors, including vascular endothelial growth factor A (VEGF-A), placental growth factor (PGF), and platelet-derived growth factor (PDGF), have been detected in the inflamed mucosa and the blood of patients with active disease (7, 10–12). However, experimental colitis models have provided conflicting results on the contribution of angiogenesis to disease activity. Neutralization of VEGF-A resulted in a decreased vessel density and improvement of the disease in dextran sulfate sodium–induced (DSS-induced) and 2,4,6-trinitrobenzene sulfonic acid–induced (TNBS-induced) colitis (11, 13, 14). Deficiency of PGF was also associated with reduced angiogenic activity but, in contrast, failed to ameliorate colitis in the experimental models (15). These

Conflict of interest: The authors have declared that no conflict of interest exists.

Submitted: September 13, 2018; **Accepted:** August 1, 2019; **Published:** September 30, 2019.
Reference information: *J Clin Invest*. 2019;129(11):4691–4707.
https://doi.org/10.1172/JCI124884.

results indicate that other vascular-directed effects apart from pure activation of angiogenesis may be related to IBD pathogenesis. In this framework it is of interest that the vasculature in the inflamed intestine is described as tortuous, irregular, and heavily disorganized and that sporadically the absence of pericytes, vessel leakiness, or edema has been reported (7, 16, 17). Altogether, the pathophysiological role of the vasculature and its regulation in IBD remain poorly understood (7, 12). The concomitant presence of different inflammatory mediators, which also exhibit pro- and antiangiogenic activities, might disturb vascular homeostasis, accounting for the disorganization of the intestinal vasculature observed in IBD. The elucidation of the respective pathomechanisms could open new insights into the mechanisms of vessel-dependent regulation of inflammation and provide new approaches for therapeutic intervention in IBD.

One of the most highly upregulated cytokines in IBD and mouse models of intestinal inflammation is interferon-γ (IFN-γ) (4, 18–25). During DSS-induced experimental colitis in mice, robust IFN-γ production in the gut has been observed. *IFN-γ*$^{-/-}$ mice showed decreased DSS-induced inflammation, indicating an indispensable role of this cytokine in colitis initiation, and establishing the DSS-colitis model as an appropriate model to study IFN-γ pathogenic effects (19, 24, 25). The pathophysiological role of IFN-γ in IBD has been attributed to its immune-modulatory or epithelial effects (4, 24). However, studies from our laboratory and others demonstrated that IFN-γ also exerts potent activities on the vasculature. In vitro, IFN-γ exhibited antiangiogenic effects by inhibiting proliferation, migration, invasion, and tube formation of endothelial cells, while increasing the permeability of endothelial cell monolayers (22, 26–30). Moreover, the activation of blood vessels by IFN-γ could be detected in human tissues by the expression of guanylate-binding protein 1 (GBP-1) in the inflamed mucosa during IBD and in colorectal carcinoma (25, 31). In colorectal carcinoma, tumor vessel activation by IFN-γ was associated with intratumoral angiostasis and improved prognosis of the patients (25, 31). Most interestingly, blockade of IFN-γ by a specific antibody resulted in increased vessel density and reduced vessel permeability in a DSS-induced colitis mouse model (25). The latter supports the pathogenetically relevant vessel-directed activities of IFN-γ in IBD. However, IFN-γ is a pleiotropic cytokine, and inhibition of IFN-γ in DSS-colitis might affect multiple different activities of the cytokine on various cell types (32). Therefore, in the present study, we investigated the vascular-specific effects of IFN-γ in vivo, their contribution to the pathogenesis of IBD, and perspectives on the vascular system as a novel target for treatment of this disease.

Results

Endothelial-specific inhibition of the IFN-γ response ameliorates DSS-induced colitis in mice. To analyze the impact of vessel-directed effects of IFN-γ in the pathogenesis of IBD, 2 different endothelial cell–specific IFN-γ receptor 2–knockout mouse models were generated. The first model (referred to as Ifngr2$^{\Delta EC}$) was generated by cross-breeding of mice with floxed *Ifngr2* alleles and mice expressing the Cre recombinase under the control of the promoter of angiopoietin receptor 2 (*Ifngr2*$^{fl/fl}$ × *Tie-2-Cre* mice; for genotype, see Supplemental Figure 1, A and B; supplemental material available online with this article; https://doi.org/10.1172/JCI124884DS1) (33). The second model (referred to as Ifngr2$^{i\Delta EC}$) was based on an inducible gene knockout generated by cross-breeding of *Ifngr2*$^{fl/fl}$ mice with mice expressing a tamoxifen-inducible Cre recombinase driven by the cadherin 5 promoter (synonym: vascular endothelial cadherin [VE-cadherin]) (*Ifngr2*$^{fl/fl}$ × *Cdh5-CreERT2* mice (34); for genotype, see Supplemental Figure 1C). Littermates with floxed *Ifngr2* alleles (*Ifngr2*$^{fl/fl}$) were used as controls in all experiments. Deletion of *Ifngr2* in Ifngr2$^{\Delta EC}$ mice was confirmed at the mRNA level in isolated lung endothelial cells (Supplemental Figure 2A). Since *Tie2* is also expressed in hematopoietic cells during development (35), *Ifngr2* was also downregulated in isolated bone marrow cells (Supplemental Figure 2B). To compensate for the inhibition of *Ifngr2* expression in hematopoietic cells, both Ifngr2$^{\Delta EC}$ and control mice were subjected to bone marrow transplantation with wild-type bone marrow cells before the experiments to exchange the hematopoietic cells (Supplemental Figure 2, C and D). Phenotyping of common immune cell subsets by flow cytometry revealed no impact of the *Ifngr2* knockout on the immune system of the mice at steady state (Supplemental Figure 2E). Gene knockout in tamoxifen-treated Ifngr2$^{i\Delta EC}$ mice was endothelial cell–specific and did not require further processing. Endothelial cell–specific knockout of IFN-γ receptor 2 in Ifngr2$^{\Delta EC}$ and Ifngr2$^{i\Delta EC}$ animals was confirmed by immunohistochemical staining (Figure 1A). In order to exclude that the *Tie-2-Cre* mouse model did lead to unintended recombination in nontargeted cell types, which may lead to a gene knockout in the whole organism of the offspring (36), we confirmed that *Ifngr2* expression was not compromised in the epithelial cells of the Ifngr2$^{\Delta EC}$ mice used in this study (Supplemental Figure 3).

Subsequently acute colitis was induced by treatment of the mice with 2.5% DSS, and the course of disease was monitored by mini-endoscopy. Colitis severity was evaluated by an endoscopic score based on thickening of the colon wall, changes in the normal vascular pattern, the presence of fibrin, mucosal granularity, and stool consistency according to Becker et al. (37). Ifngr2$^{\Delta EC}$ and Ifngr2$^{i\Delta EC}$ mice showed a significantly lower endoscopic score than control mice, indicating that inhibition of the vascular IFN-γ response ameliorates acute DSS-induced colitis (Figure 1B). Moreover, these results could be confirmed in a chronic colitis model using Ifngr2$^{\Delta EC}$ mice and 3 cycles of DSS treatment (Figure 1B, bottom). In agreement with the reduced inflammation, colon length was increased in the Ifngr2$^{\Delta EC}$ and Ifngr2$^{i\Delta EC}$ mice relative to the control mice after DSS treatment, under conditions of both acute and chronic colitis (Figure 1C). Furthermore, the tissue architecture of the resected colon was less disrupted and showed fewer signs of inflammation in Ifngr2$^{\Delta EC}$ and Ifngr2$^{i\Delta EC}$ mice compared with the controls (Figure 1D). Immunofluorescence staining of the general lymphocytic marker CD45 and the macrophage marker F4/80 exhibited a reduced immune cell infiltration into the colonic tissue in Ifngr2$^{\Delta EC}$ and Ifngr2$^{i\Delta EC}$ mice after acute and chronic DSS treatment compared with the control group (Figure 2, A and B). Identical results were obtained by staining with the T cell marker CD4 (Supplemental Figure 4). Altogether, these results demonstrate that the vascular-directed effects of IFN-γ are crucial drivers of DSS-induced experimental colitis.

IFN-γ exerts angiostatic activities during DSS-induced colitis. Previous studies have shown that IFN-γ can inhibit angiogenesis

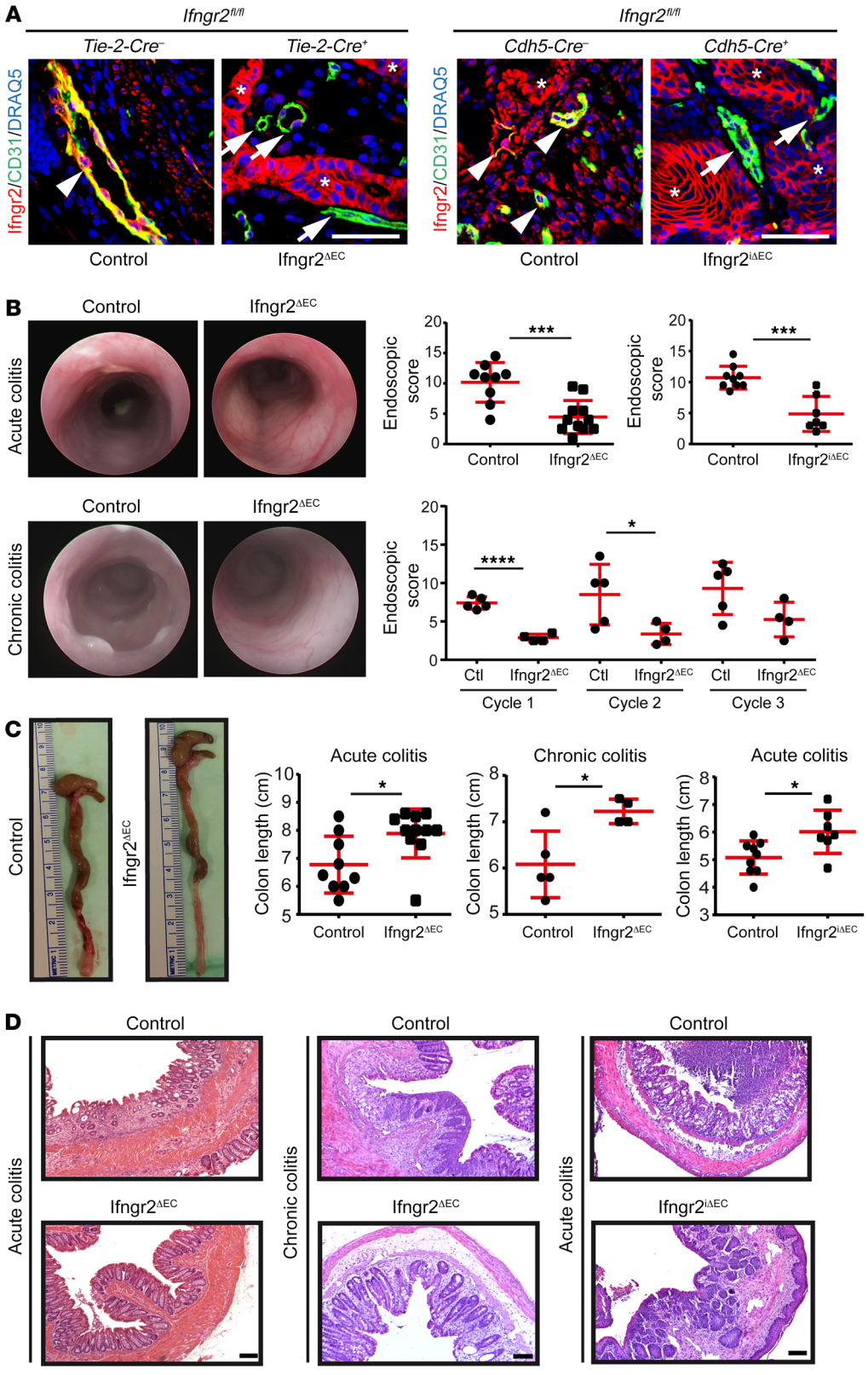

Figure 1. Endothelial-specific inhibition of the IFN-γ response ameliorates DSS-induced colitis in mice. Mice with an endothelial cell–specific knockout of IFN-γ receptor 2 either from onset ($Ifngr2^{\Delta EC}$, $n = 11$) or after tamoxifen induction ($Ifngr2^{i\Delta EC}$, $n = 7$) and mice with floxed Ifngr2 alleles (Control, both $n = 9$) were compared. Colitis was induced by addition of 2.5% DSS to the drinking water for either 1 cycle (acute colitis) or 3 cycles (chronic colitis, 4 $Ifngr2^{\Delta EC}$ and 5 $Ifngr2^{fl/fl}$). (**A**) Endothelial cell–specific knockout of the receptor was analyzed by immunofluorescent costaining of IFN-γ receptor 2 (red) and the endothelial cell marker CD31 (green). A strong expression of the receptor in colon epithelial cells was maintained in all animals (asterisks). The receptor was absent in endothelial cells of knockout animals (green, arrows) and present in colon vessels of control animals (yellow, arrowheads). Nuclei were stained with DRAQ5 (blue). Scale bars: 50 μm. (**B**–**D**) Colon inflammation was analyzed by endoscopic score (**B**), measurement of colon length (**C**), and histologic examination after H&E staining (**D**). Scale bars: 100 μm. Representative pictures are shown. All graphs represent data quantification with means ± SD. Two-tailed, unpaired Student's *t* test (**B** and **C**) was used to determine statistical significance (*$P < 0.05$, ***$P < 0.001$, ****$P < 0.0001$).

in vitro (28–30). We confirmed the antiangiogenic effects of IFN-γ under flow conditions using a microfluidic 3D coculture model of human umbilical vein endothelial cells (HUVECs) and fibroblasts (38, 39). IFN-γ treatment significantly reduced endothelial cell sprout length and thickness (Figure 3A).

In order to determine whether IFN-γ is also able to inhibit angiogenesis in complex murine cell culture models, the metatarsal sprouting assay was used (40). Metatarsal bones from both $Ifngr2^{\Delta EC}$ and control embryos were isolated at gestational day 18.5, put in culture, and stimulated with VEGF-A to

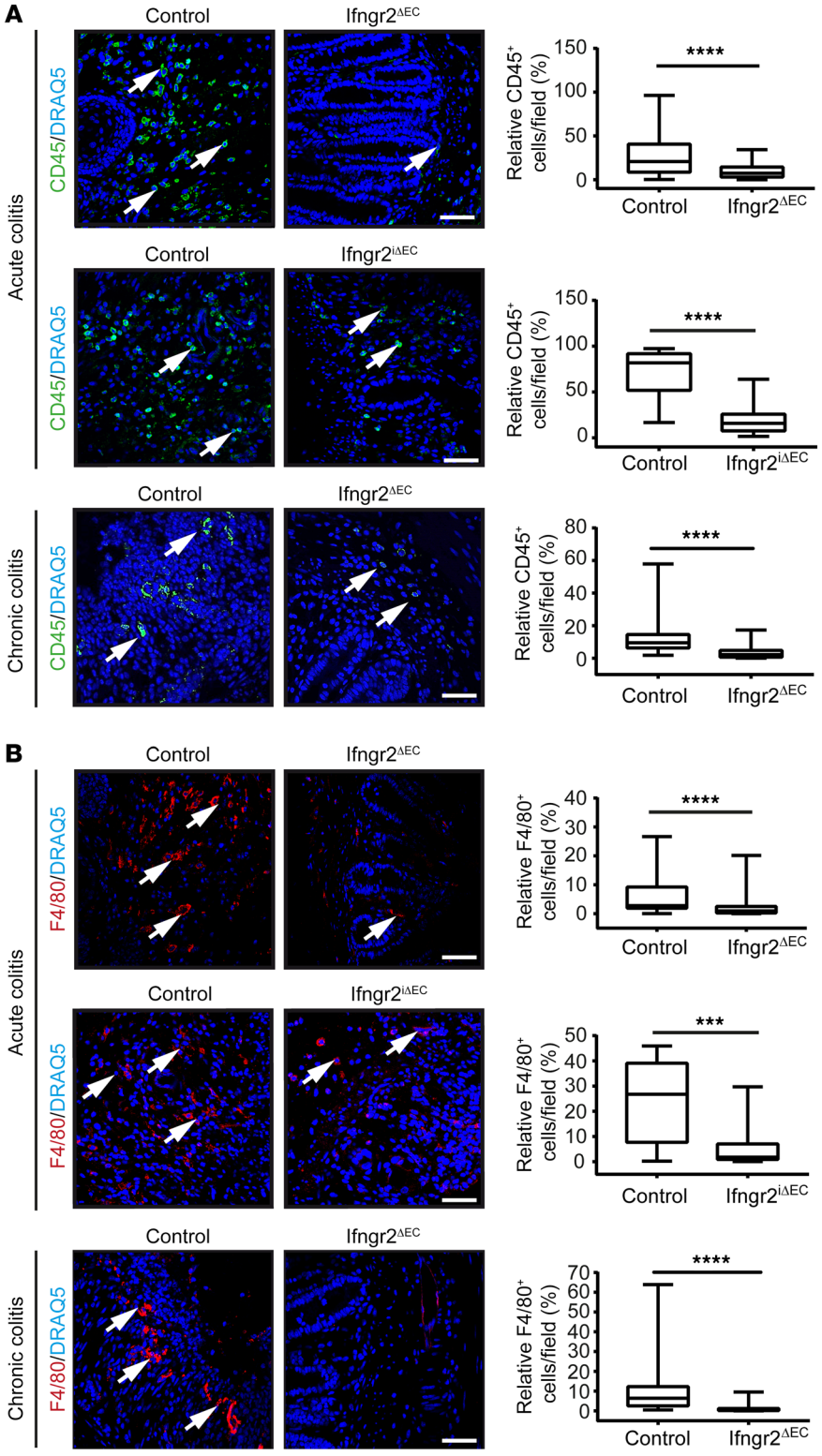

Figure 2. Endothelial-specific inhibition of the IFN-γ response suppresses immune cell infiltration during DSS-induced colitis in mice. Mice with an endothelial cell–specific knockout of IFN-γ receptor 2 (Ifngr2$^{\Delta EC}$; Ifngr2$^{i\Delta EC}$) and mice with floxed Ifngr2 alleles (Control) were compared. Colitis was induced by addition of 2.5% DSS to the drinking water for either 1 cycle (acute colitis) or 3 cycles (chronic colitis). Colonic immune cell infiltration was determined by immunofluorescence staining of CD45 (green) (**A**) and F4/80 (red) (**B**). Nuclei were stained with DRAQ5 (blue). Arrows indicate examples for CD45$^+$ or F4/80$^+$ cells (left panels). Scale bars: 50 μm. Quantitative evaluations are shown on the right side of each panel, including the pooled results from 2 independent experiments (in the acute DSS-colitis model, 11 Ifngr2$^{\Delta EC}$ mice were compared with 9 control mice and 5 Ifngr2$^{i\Delta EC}$ mice with 3 control mice; in the chronic colitis model, 4 Ifngr2$^{\Delta EC}$ mice were compared with 5 control mice). Representative pictures are shown. Data are expressed as box-and-whisker plots. Horizontal bars indicate the median, box borders indicate the 25th and 75th percentiles, and whiskers indicate minimum and maximum values. Mann-Whitney *U* test (**A** and **B**) was used to determine statistical significance (***$P < 0.001$, ****$P < 0.0001$).

induce vessel sprouting (Figure 3B). IFN-γ completely inhibited VEGF-A–induced angiogenic sprouting in metatarsal bones of control animals but not of Ifngr2$^{\Delta EC}$ animals, confirming the angiostatic role of IFN-γ in mice (Figure 3B). Next, the influence of IFN-γ on angiogenesis in vivo during acute colitis was examined by immunofluorescence staining of the endothelial cell marker CD31 and the proliferation marker Ki-67 (Figure 3C). During DSS-induced colitis, vessel density and vessel proliferation rates were significantly increased in colon tissues of Ifngr2$^{\Delta EC}$ mice relative to control mice. These results demonstrate that inflammation-induced angiogenesis is repressed by IFN-γ in DSS-induced experimental colitis.

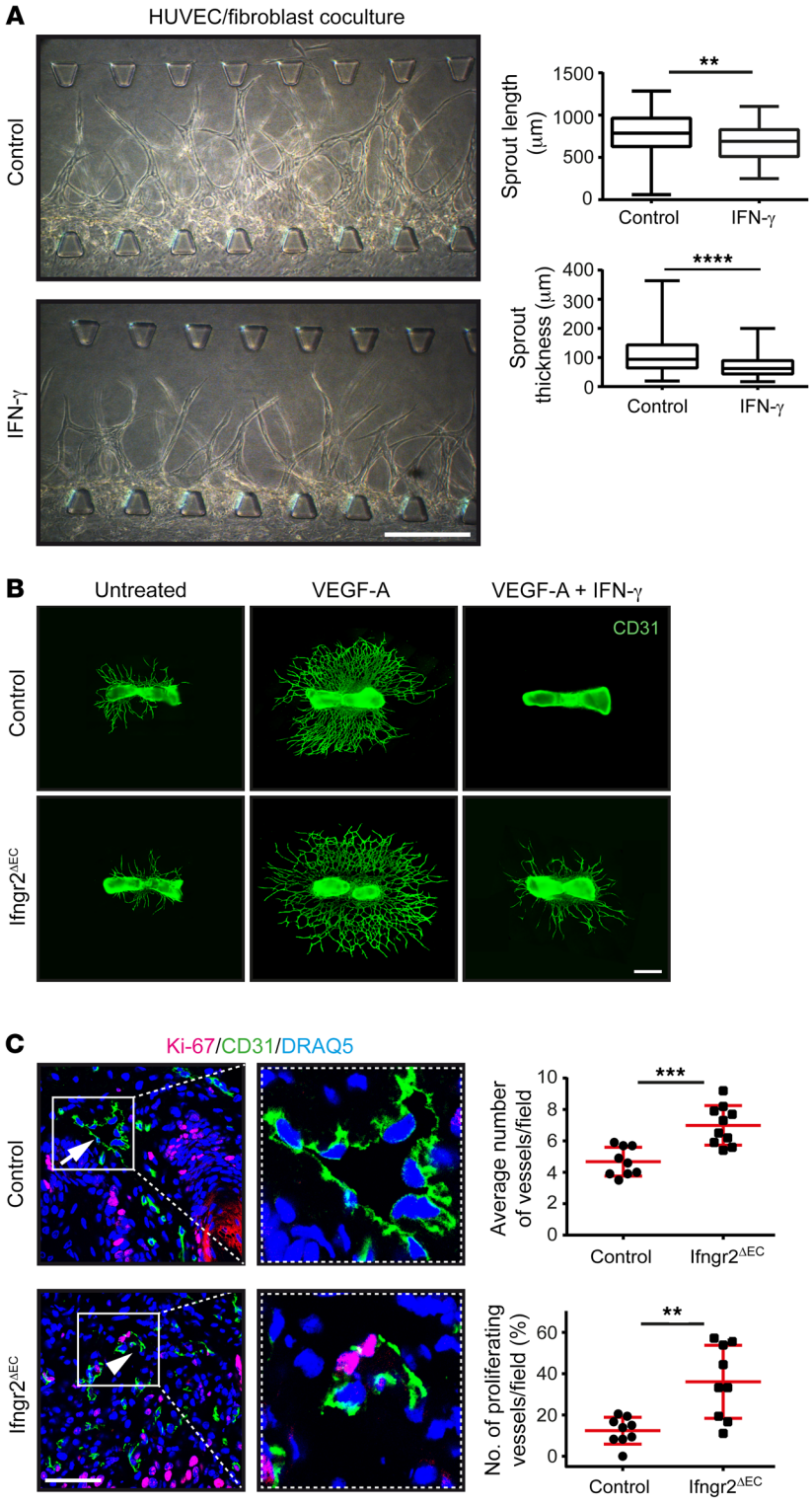

Figure 3. IFN-γ exerts angiostatic effects in vitro, ex vivo, and in vivo. (**A**) In vitro angiogenesis on a 3D microfluidic chip using HUVEC and fibroblast cocultures. Representative pictures are shown. IFN-γ significantly reduced angiogenic sprout length and thickness. Scale bar: 300 μm. Quantification included control (n = 9) and IFN-γ–treated (100 U/mL) chips (n = 6) with 15 sprouts analyzed per chip. (**B**) Metatarsals of 18.5-day-old mouse embryos after 10 days of cultivation. Ex vivo vessel outgrowth was visualized by immunofluorescence staining (CD31, green). Vessel outgrowth stimulated by VEGF-A (100 ng/mL) was completely inhibited by IFN-γ (100 U/mL) in control but not in Ifngr2$^{\Delta EC}$ mice. One representative picture of 5 experiments is shown. Scale bar: 500 μm. (**C**) Representative images of colon tissue from control and Ifngr2^{EC} mice with DSS-colitis double-stained for CD31 (green) and Ki-67 (pink). Counterstaining was performed with DRAQ5 (blue). The arrow indicates an example of a nonproliferating vessel, whereas the arrowhead points to a proliferating vessel. Scale bar: 50 μm. Vessel number (CD31$^+$ with lumen) was counted in 10 regions per section (n = 9 control mice; n = 10 Ifngr2$^{\Delta EC}$ mice). Ki-67$^+$ vessels were counted as angiogenic vessels, and 162 vessels per group were analyzed in total (n = 9 control mice; n = 9 Ifngr2$^{\Delta EC}$ mice). Quantification included pooled results from 2 independent experiments (right panels). Data are expressed as box-and-whisker plots (horizontal bars, median; box borders, 25th and 75th percentiles; whiskers, minimum and maximum values) (**A**) or as means ± SD (**C**). Two-tailed, unpaired Student's t test (**A**, length; **C**, vessel number) and Mann-Whitney U test (**A**, thickness; **C**, vessel proliferation) were used to determine statistical significance (**P < 0.01, ***P < 0.001, ****P < 0.0001).

Angiogenesis is not related to the pathogenesis of DSS-induced colitis in mice. During DSS-induced colitis in Ifngr2$^{\Delta EC}$ mice, disease activity was reduced, and angiogenic activity was increased in comparison with control animals, suggesting that the course of IBD pathogenesis might be inversely related to the angiogenic activity. To further investigate the relation of angiogenesis and IBD pathogenesis, we compared the course of DSS-colitis under conditions of angiogenesis inhibition (control mice treated with the VEGF-A–neutralizing antibody B20-4.1.1) (41, 42) and angiogenesis activation (Ifngr2$^{\Delta EC}$ mice receiving an isotype antibody). Control mice receiving an isotype antibody were included as a further control. Functional validation of the antibodies in vitro showed that the anti–VEGF-A but not the isotype antibody inhibited VEGF-A–induced proliferation of primary mouse intestinal endothelial cells

(MIECs) (Supplemental Figure 5A). In accordance with this, vessel density and vessel proliferation in the DSS-induced colitis model were lowest in the colon of animals treated with the anti–VEGF-A antibody and highest in the Ifngr2$^{\Delta EC}$ mice treated with the isotype antibody (Figure 4A and Supplemental Figure 5B). In unchallenged Ifngr2$^{\Delta EC}$ and control mice, colon vessel density and proliferation were equally low (Supplemental Figure 5C).

However, unrelated to angiogenic activity, DSS-induced colitis was significantly reduced in both control mice with anti–VEGF-A treatment and Ifngr2$^{\Delta EC}$ mice treated with the isotype antibody, but remained high in control mice treated with the isotype antibody (Figure 4, B–D). This was based on endoscopic evaluation of inflammation (Figure 4B), colon length measurement (Figure 4C), and histologic analysis of the crypt architecture (Figure 4D). Accordingly, reduced lymphocytic cell infiltration (CD45$^+$) into colonic tissue was observed for control mice treated with the anti–VEGF-A antibody and Ifngr2$^{\Delta EC}$ mice treated with the isotype antibody (Figure 4E). These results demonstrate that the course of IBD pathogenesis was not related to angiogenesis and may depend on other functions of IFN-γ–induced vessel activation.

The intestinal vasculature is characterized by IFN-γ–mediated barrier dysfunction in experimental colitis in mice and human IBD patients. The results presented so far suggest that vascular effects of IFN-γ — other than its angiostatic functions — are involved in IBD pathogenesis. As previous studies have indicated that IFN-γ increases vessel permeability (22, 25, 26), the pathogenesis-related impact of IFN-γ on the intestinal vascular barrier function was investigated. To achieve this, we performed intravital imaging of the vessels in colon crypts. The intestinal vasculature was visualized by detection of 70-kDa FITC-dextran injected i.v. into Ifngr2$^{\Delta EC}$, Ifngr2$^{i\Delta EC}$, and control mice undergoing acute DSS-induced colitis and Ifngr2$^{\Delta EC}$ with chronic DSS-induced colitis. The accumulation of FITC-dextran in the lumen of intestinal crypts indicated vessel permeability. Relative permeability was calculated as the ratio of FITC signal inside the crypts over the total FITC signal. Applying this measurement, vessel permeability was found to be decreased in all *Ifngr2*-knockout mice, in both acute and chronic disease, as compared with control mice (Figure 5, A–C). Notably, vascular permeability was also significantly decreased in control mice treated with the VEGF-A–neutralizing antibody (Figure 5D) but was not compromised in unchallenged Ifngr2$^{\Delta EC}$ and control mice (Supplemental Figure 6A). Since both the deletion of IFN-γ receptor 2 and anti–VEGF-A treatment resulted in a milder course of the disease in mice (Figure 4, B–E), we reasoned that the vascular barrier integrity was functionally linked to the pathogenesis of DSS-induced experimental colitis.

To investigate whether differential barrier integrity can also be confirmed at the low–molecular weight level, cadaverine (0.86 kDa) was used as an additional fluorescent permeant and analyzed by light-sheet microscopy (Supplemental Figure 6B). The vasculature was contrasted with lectin staining. Calculating the ratio of cadaverine fluorescence intensity detected outside the vessels over the total cadaverine signal confirmed that Ifngr2$^{\Delta EC}$ and control mice also exhibited differential vascular barrier integrity in acute DSS-colitis at the low–molecular weight level (Supplemental Figure 6B; for 3D visualization, see Supplemental Figure 7 and its accompanying video). Taken together, these data show that IFN-γ impairs the vascular barrier function in vivo during DSS-induced colitis in a pathogenesis-associated manner.

Next, we assessed the clinical relevance of our finding. Intestinal vascular leakage was analyzed by probe-based confocal laser endomicroscopy (pCLE) after fluorescein infusion in a cohort of 15 IBD patients either in remission (n = 7) or in an active disease state (n = 8). As a control, patients without IBD undergoing confocal endoscopy for other diagnostic reasons were used (n = 3; for clinical patients' characteristics, see Supplemental Table 1). In striking analogy to the mouse models, increased permeability of the human colonic vessels led to extravasation and detection of the fluorescein signal in the intestinal crypts (Figure 5E). The calculated ratio of fluorescein signal inside the crypts over the total fluorescein signal was used as a relative measure of vascular leakage. Vessel permeability was significantly increased in IBD patients with active disease relative to patients in disease remission or control persons without IBD (Figure 5E). Collectively, these data confirm the pathogenic importance of vascular leakiness in IBD.

IFN-γ compromises mural cell coverage and VE-cadherin–mediated cell-cell interactions during colitis-associated vascular barrier breakdown. The key components of vascular barrier integrity are vessel maturation, as indicated by mural cell coverage of vessels, and endothelial cell-cell interactions (43–46). To investigate the impact of the vascular IFN-γ response on differential mural cell coverage of vessels in DSS-induced colitis, costaining of CD31 and α-smooth muscle actin (α-SMA) or PDGF receptor-β (PDGFR-β) was performed in resected colon tissues of Ifngr2$^{\Delta EC}$ and control mice. We observed a general upregulation of the expression of PDGFR-β in many different cells (most likely fibroblasts) in inflamed tissues as compared with noninflamed tissues (Supplemental Figure 8). Accordingly, it was difficult to determine whether vessel-associated expression was derived from pericytes or other cells in close proximity, and we focused on α-SMA for the detection of mural cells. Quantitative analyses of α-SMA–derived results demonstrated high mural cell coverage in 57% of vessels from Ifngr2$^{\Delta EC}$ mice but in only 30% of vessels from control mice with DSS-induced colitis (Figure 6A, black area).

Endothelial cell-cell interactions critically depend on adherens junction VE-cadherin. VE-cadherin extracellular domains exposed on the surface of adjacent endothelial cells form homodimeric interactions leading to the tight connection of the cell membranes (43). Loss of VE-cadherin integrity is commonly associated with increased vascular permeability (47). We investigated whether VE-cadherin might also be impaired during IFN-γ–induced vascular leakiness in DSS-induced colitis. Two-photon microscopy was used to visualize mouse colon vasculature (CD31 immunofluorescence staining) and VE-cadherin in high-resolution 3D imaging. VE-cadherin was stained with an antibody recognizing its extracellular domain to specifically detect parts of the molecule involved in cell-cell contacts. Control mice with acute DSS-induced colitis showed an irregular and tortuous vascular network associated with a loss of VE-cadherin integrity at cell-cell junctions (Figure 6B). On the contrary, Ifngr2$^{\Delta EC}$ mice displayed a regular vascular network associated with continuous VE-cadherin structures. Accordingly, colocalization of VE-cadherin with CD31 was significantly reduced by roughly 40% in control mice as compared with Ifngr2$^{\Delta EC}$ mice

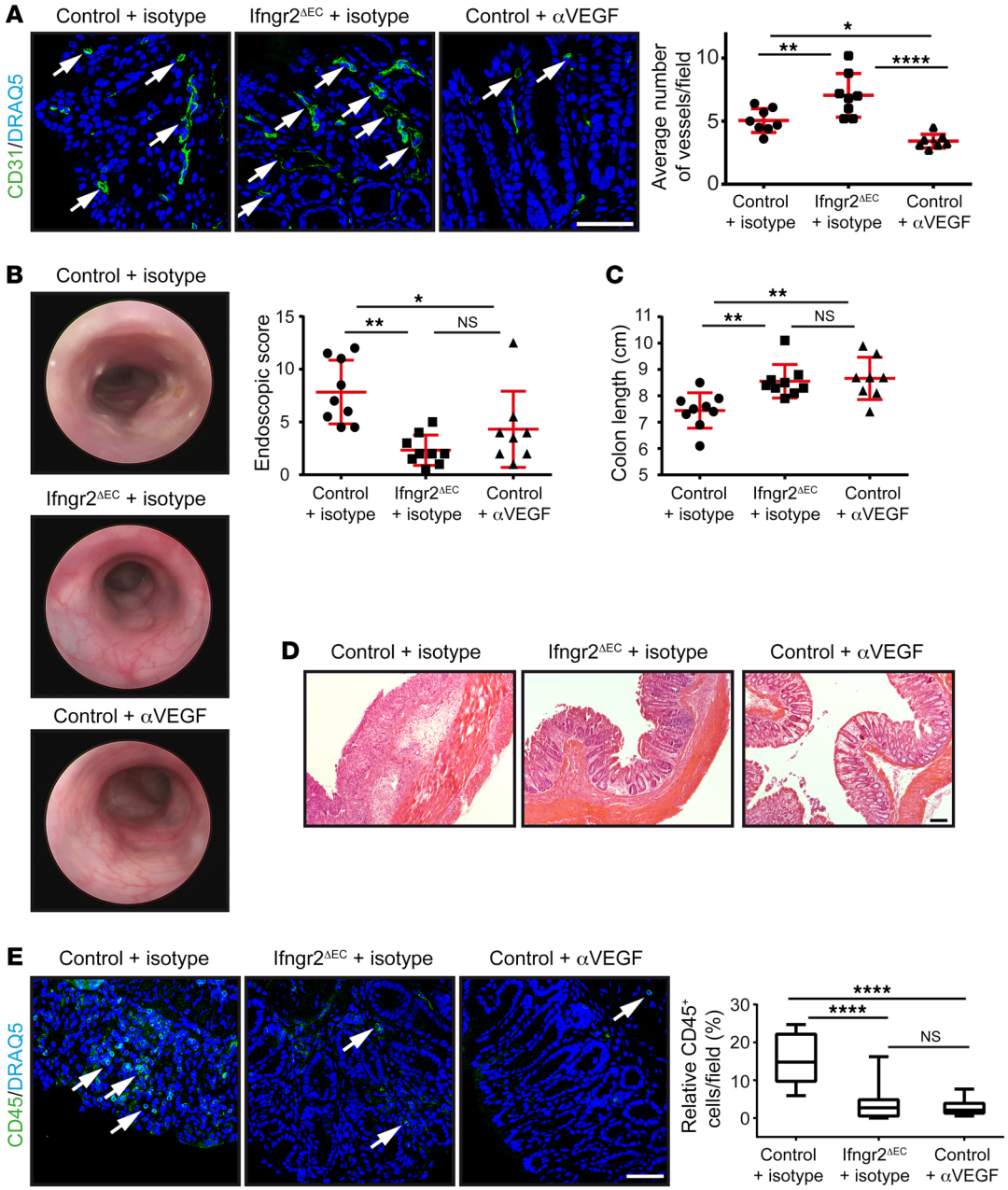

Figure 4. Angiogenesis is not related to the pathogenesis of DSS-induced colitis in mice. During DSS-colitis, control mice were injected either with a monoclonal antibody (B20-4.1.1, 150 μg/mouse) blocking the interaction of VEGF-A with VEGF receptors 1 and 2 (αVEGF; $n = 8$) or with an isotype antibody (150 μg/mouse, $n = 9$) and were compared with Ifngr2$^{\Delta EC}$ mice receiving the isotype antibody ($n = 9$). (**A**) Vessel number (CD31, green) was counted in 10 regions per colon tissue section. Arrows indicate CD31$^+$ vessels with lumen. Scale bar: 50 μm. (**B**–**D**) Colitis grade was evaluated by endoscopic score (**B**), colon length (**C**), histologic presentation after H&E staining (scale bar: 100 μm) (**D**), and CD45 immune cell infiltration (green, arrows), analyzed in 5 regions per colon tissue section (scale bar: 50 μm) (**E**). Representative pictures are shown. Quantitative evaluations are shown on the right side of the respective panels, including the pooled results from 2 independent experiments. Graphs present means ± SD (**A**–**C**) or box-and-whisker plots, where horizontal bars indicate the median, box borders indicate the 25th and 75th percentiles, and whiskers indicate minimum and maximum values (**E**). One-way ANOVA followed by Tukey's post hoc test (**A**, **B**, and **E**) and Kruskal-Wallis test followed by Dunn's post hoc test (**C**) were used to determine statistical significance (*$P < 0.05$, **$P < 0.01$, ****$P < 0.0001$). Genotypes of respective mice are shown in Supplemental Figure 1D.

with DSS-induced colitis (Figure 6B; for 3D visualization, see Supplemental Figure 9 and its accompanying video).

As intestinal vessels of human IBD patients have been described to exhibit irregular and tortuous structures (16, 17), we investigated whether this might also be associated with a loss of VE-cadherin integrity. The quantitative evaluation of VE-cadherin colocalization with vessels from highly inflamed regions and corresponding uninvolved tissues of human IBD patients showed that vessels without membrane VE-cadherin expression are more common in the inflamed tissues compared with uninvolved tissues (Figure 6C, light gray areas of bars; patients' characteristics are listed in Supplemental Table 2). These results indicate that VE-cadherin

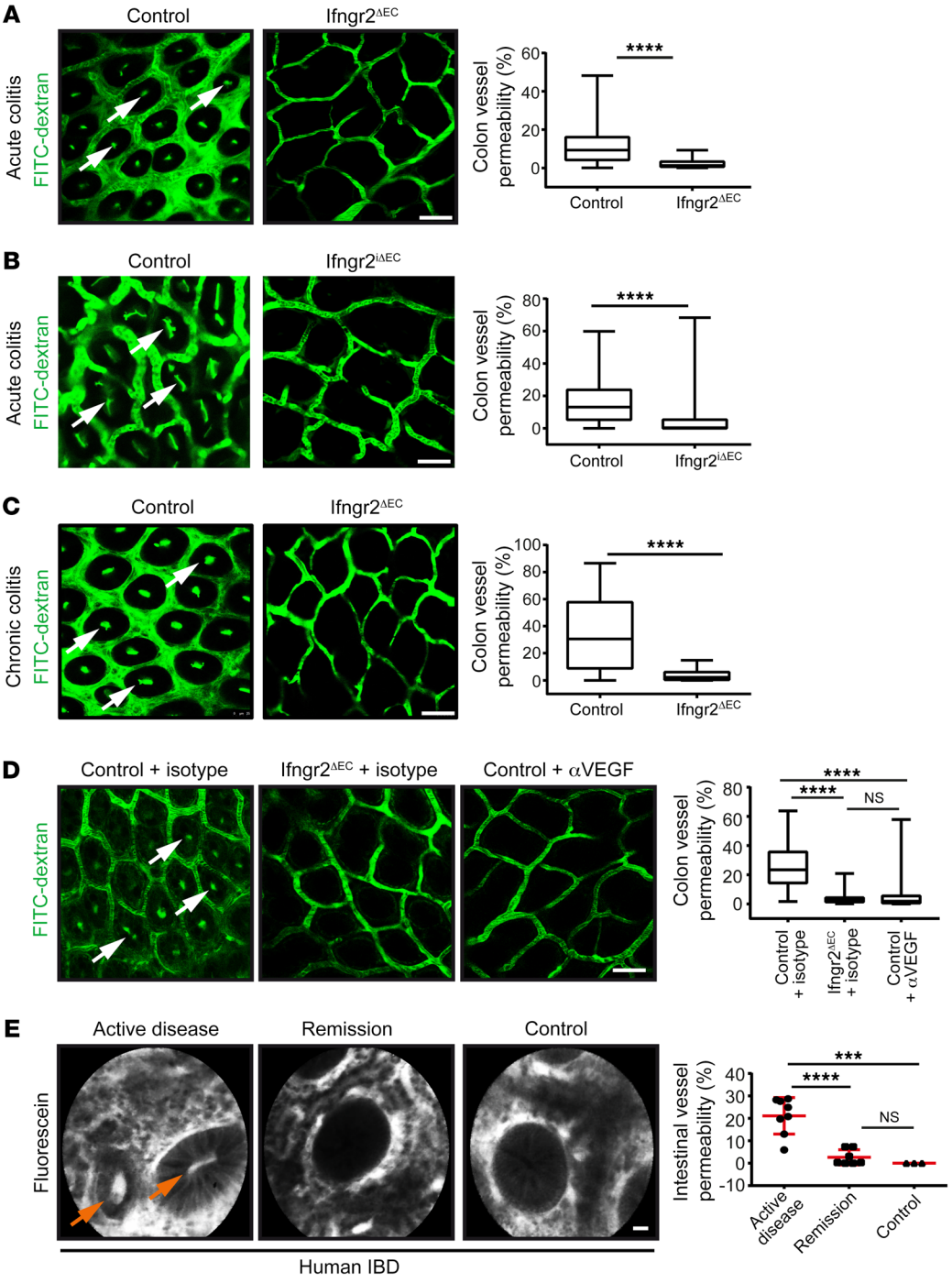

Figure 5. The intestinal vasculature is characterized by IFN-γ–mediated barrier dysfunction in murine DSS-induced colitis and human IBD. (**A**–**D**) Seventy-kDa FITC-dextran (10 mg/mL) was injected i.v. in mice with acute and chronic DSS-colitis. Accumulation in intestinal crypts (arrows) indicates vessel permeability, calculated as the ratio of FITC signal inside the crypts over the total FITC signal. Vessel permeability was reduced in Ifngr2$^{\Delta EC}$ (n = 4) (**A**) and Ifngr2$^{i\Delta EC}$ (n = 7) mice (**B**) compared with control mice (n = 4 and 7, respectively) during acute (**A** and **B**) and chronic colitis (**C**; 4 Ifngr2$^{\Delta EC}$ vs. 5 control). For quantitative evaluation, 10–12 crypts were analyzed per mouse. Scale bars: 50 μm. (**D**) Control mice with αVEGF treatment (150 μg/mouse, n = 8) and Ifngr2$^{\Delta EC}$ mice (n = 8) showed reduced vascular permeability in contrast to control mice treated with isotype antibody (150 μg/mouse, n = 7). Scale bar: 50 μm. For quantitative evaluation, 10 crypts per mouse were analyzed. Pooled results from 2 independent experiments are shown. (**E**) Human IBD patients with active disease (n = 8) or remission (n = 7) or control patients without IBD (n = 3) underwent pCLE. Fluorescein accumulation in intestinal crypts (arrows) indicates vessel permeability, calculated as the ratio of fluorescein signal inside the crypts over total fluorescein signal. Vessel permeability was increased in active disease (10 crypts per patient). Scale bar: 20 μm. Representative pictures are shown. Quantitative evaluations (right side of each panel) are shown as box-and-whisker plots (horizontal bars, median; box borders, 25th and 75th percentiles; whiskers, minimum and maximum values; **A**–**D**) or means ± SD (**E**). Mann-Whitney U test (**A**–**C**), Kruskal-Wallis test followed by Dunn's post hoc test (**D**), and 1-way ANOVA followed by Tukey's post hoc test (**D**) were used to determine statistical significance (***P < 0.001, ****P < 0.0001).

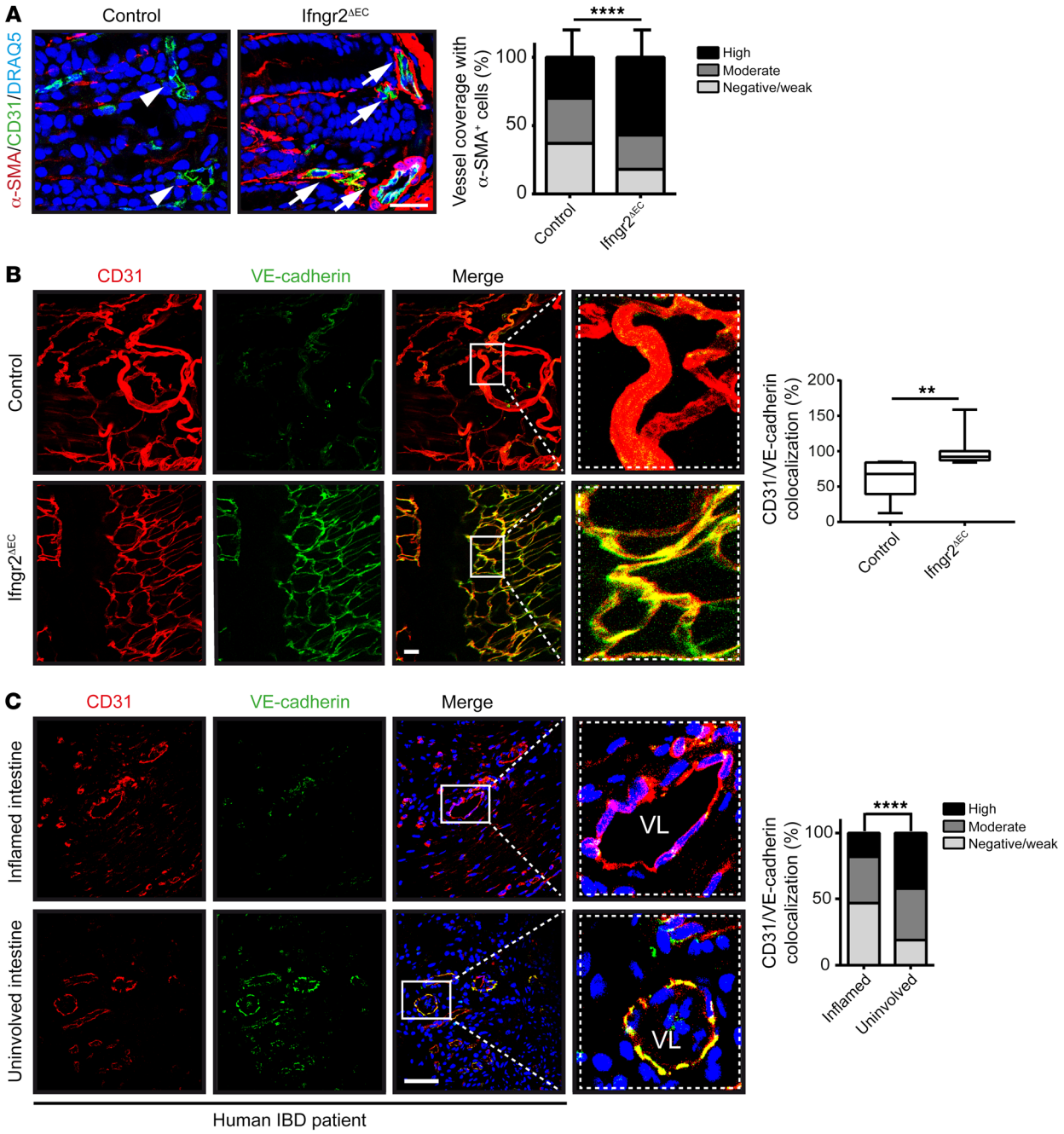

Figure 6. IFN-γ compromises mural cell coverage and VE-cadherin–mediated cell-cell interactions during DSS-induced colitis and human IBD. (**A**) Costaining of α-SMA (red) and CD31 (green) in colon tissue of Ifngr2$^{\Delta EC}$ (n = 11, in total 783 vessels) and control mice (n = 9, in total 827 vessels) with DSS-colitis (pooled results from 2 independent experiments). Mural cell coverage (α-SMA$^+$) was categorized as negative/weak (arrowheads), moderate, or high (arrows). Scale bar: 25 μm. (**B**) VE-cadherin (green) colocalization with colonic vessels (CD31, red) of Ifngr2$^{\Delta EC}$ and control mice with DSS-colitis (n = 3 each) visualized by 2-photon microscopy. The mean colocalization of Ifngr2$^{\Delta EC}$ mice was set to 100%. Data are expressed as box-and-whisker plots. Horizontal bars indicate the median, box borders indicate the 25th and 75th percentiles, and whiskers indicate minimum and maximum values. Scale bar: 25 μm. (**C**) Human IBD and corresponding uninvolved intestinal tissues (n = 11; 487 vessels in inflamed and 333 vessels in uninvolved regions) were stained for CD31 (red) and VE-cadherin (green). Vessel colocalization with VE-cadherin was categorized as negative/weak, moderate, or high. VL, vessel lumen. Scale bar: 50 μm. (**A** and **C**) Nuclei stained by DRAQ5 (blue). χ^2 test (**A** and **C**) and 2-tailed, unpaired Student's t test (**B**) were used (**P < 0.01, ****P < 0.0001).

expression and function are impaired in acute inflammation in IBD, supporting the clinical relevance of our findings.

The direct impact of IFN-γ on VE-cadherin was investigated with HUVECs in the microfluidic 3D vasculogenesis chip in vitro model (38, 39). Vascular networks treated with IFN-γ were characterized by the disassembly of membrane VE-cadherin structures at cell-cell contacts in comparison with untreated cells, which exhibited continuous membrane-associated VE-cadherin staining at cell-cell contact areas (Figure 7A). These results were confirmed with MIECs under static conditions. While untreated

MIECs exhibited a linear VE-cadherin pattern at the membrane, IFN-γ–treated cells lacked membranous VE-cadherin and were characterized by perinuclear aggregations of VE-cadherin (Figure 7B, asterisks). VEGF-A, which is known to disrupt the VE-cadherin membrane pattern and to increase internalization (48), was used as a control. VEGF-A interrupted VE-cadherin localization at the membrane and induced internalization of VE-cadherin (Figure 7B, asterisks), but this was less prominent than seen with IFN-γ. Combined treatment of MIECs with both IFN-γ and VEGF-A resulted in almost complete VE-cadherin disruption at the membrane (Figure 7B).

Previous studies suggested that mechanisms modulating the organization of junctions, for example through their internalization, specifically target VE-cadherin (49). Therefore, we investigated the expression and localization of the tight junction protein zonula occludens-1 (ZO-1) (45) to determine whether the IFN-γ effects are specific for the adherens junction or also affect tight junction proteins. In MIECs treated with IFN-γ, cell membrane–associated distribution of VE-cadherin was disrupted, whereas ZO-1 was still associated with the cell membrane in the same cells (Figure 7C). This suggested that adherens junctions with VE-cadherin are the specific target of barrier-directed activities of IFN-γ.

To assess whether the loss of VE-cadherin junctions is sufficient to increase endothelial permeability, Transwell permeability studies were carried out with MIECs using FITC-dextran as permeant. An anti–VE-cadherin antibody (mAbBV13), which binds to the extracellular domain of VE-cadherin and blocks homotypic adhesion and clustering at cell-cell contacts, was used to impair VE-cadherin functions (47, 49). The BV13 antibody efficiently blocked VE-cadherin clustering at cell-cell contacts, as shown by immunofluorescence staining of VE-cadherin (Figure 7D). Transwell permeability analyses confirmed that treatment with the BV13 antibody increased the permeability of MIEC monolayers as compared with cells treated with an isotype antibody or left untreated (Figure 7E). Altogether, these results demonstrate that impairment of VE-cadherin is sufficient to explain IFN-γ–associated defects of the vascular barrier.

Treatment with imatinib restores vascular barrier function and reduces DSS-induced inflammation. Imatinib is a protein tyrosine kinase inhibitor that is commonly applied as an anticancer medication, especially for chronic myelogenous leukemia, acute lymphocytic leukemia, and certain types of gastrointestinal stromal tumors (50). Interestingly, it was shown that imatinib regulates the endothelial barrier and restores VE-cadherin junctions in cells after thrombin stimulation (51–53). Our findings on the pathogenic relevance of vascular permeability in IBD pathogenesis suggest that imatinib might be a potential drug for treatment of the disease. Transwell permeability analyses confirmed that imatinib is able to inhibit IFN-γ–induced permeability in MIECs (Figure 8A). Immunofluorescence staining of VE-cadherin confirmed that imatinib restores VE-cadherin localization at cell-cell contacts in IFN-γ–treated MIECs (Figure 8B, arrows).

In order to substantiate the use of imatinib as a potential drug for the treatment of IBD, we investigated whether it inhibits vessel permeability and disease activity in the DSS-induced colitis mouse model. To achieve this, control and Ifngr2$^{\Delta EC}$ mice were treated with either imatinib or PBS during DSS-induced colitis. In vivo analysis of colon vascular leakage with i.v. injection of FITC-dextran showed that imatinib reduces vascular permeability during DSS-colitis in control mice to levels similar to those observed in Ifngr2$^{\Delta EC}$ mice (Figure 8C). This correlated with a milder colonic inflammation in the imatinib-treated control mice, as shown by the endoscopic score, colon length, and crypt architecture, in comparison with control mice receiving PBS only (Figure 8, D–F). Treatment with imatinib showed no additive effect with the *Ifngr2* knockout on the course of DSS-induced colitis (Figure 8, C–F), suggesting that imatinib and the endothelial cell–specific *Ifngr2* knockout both target vascular permeability.

Discussion

This study shows that a dysfunction of the vascular barrier is an important pathomechanism in IBD. Specifically, we demonstrated that the IBD-associated cytokine IFN-γ causes a breakdown of the vascular barrier through disruption of the adherens junction protein VE-cadherin and that this is a crucial driver of DSS-induced experimental colitis. Disease-associated vascular barrier dysfunction was confirmed in human IBD patients, supporting the clinical relevance of our findings. Treatment with imatinib restored adherens junctions, inhibited vascular permeability, and significantly reduced colonic inflammation in experimental colitis. Altogether, these results highlight the pathogenic impact of IFN-γ–mediated intestinal vessel activation in IBD and open new avenues for vascular-directed treatment of this disease (for graphical summary, see Figure 9).

A hallmark of IBD is the extensive release of cytokines (4, 54). Among them, IFN-γ plays a key role, as it is one of the most highly upregulated cytokines in both Crohn's disease (CD) and ulcerative colitis (UC), as well as in the related mouse models (4, 18–25). In agreement with this, IFN-γ belongs to genetically defined risk loci in IBD (55).

The majority of studies analyzing the role of IFN-γ in IBD pathogenesis focused on its effects on immune or epithelial cells (4, 24). However, our previous observations indicated that IFN-γ may also exert significant blood vessel–directed pathogenic functions in IBD (25). Analyzing the specific vascular impact in detail, we showed here that mice lacking the IFN-γ receptor in endothelial cells have a significantly milder course of acute and chronic forms of DSS-induced colitis. This demonstrates that the vascular effects of IFN-γ are a key component in the pathogenesis of colitis.

IFN-γ exerts angiostatic activity in colorectal carcinoma (27, 31), and IFN-γ–dependent angiostatic activity could be confirmed here in the DSS-induced experimental colitis model. Ifngr2$^{\Delta EC}$ mice displayed increased angiogenic activity in intestinal vessels as compared with wild-type controls. However, this was in contrast to reports indicating that angiogenesis fosters inflammation and IBD (7, 10). To solve this contradiction, we specifically analyzed the role of angiogenesis by comparing DSS-colitis in mice with either blockade of VEGF-A activity, which reduced angiogenesis, or knockout of the endothelial cell–specific IFN-γ response, which increased angiogenesis. In agreement with previous studies, anti–VEGF-A treatment decreased vessel density and improved the course of disease (11, 13, 14). However, the endothelial cell–specific IFN-γ receptor knockout also decreased intestinal inflammation, while increasing angiogenesis. These findings indicate

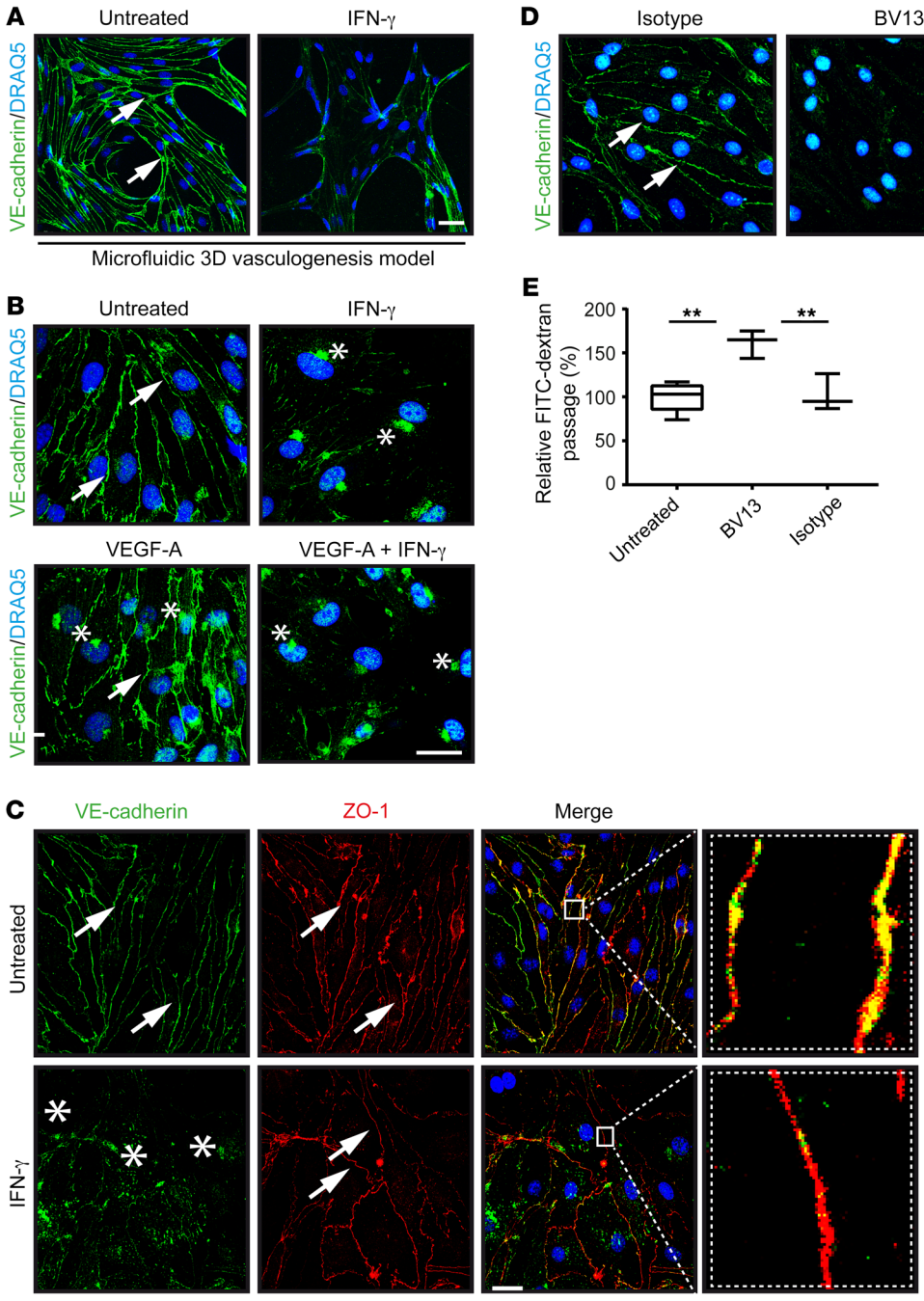

Figure 7. IFN-γ–induced disturbances of VE-cadherin–mediated cell-cell interactions are sufficient to increase vascular permeability in endothelial cells in culture. (**A** and **B**) VE-cadherin (green) localization at cell-cell contacts in a microfluidic, vasculogenic network of HUVECs (**A**; untreated, $n = 12$; IFN-γ–treated [100 U/mL], $n = 6$; scale bar: 30 μm) or in static MIECs (**B**; IFN-γ, 100 U/mL; VEGF-A, 30 ng/mL; scale bar: 25 μm). (**C**) MIECs stained for VE-cadherin (green) and ZO-1 (red) in the absence and presence of IFN-γ (100 U/mL). Scale bar: 25 μm. (**D**) VE-cadherin staining (green) in BV13-treated (50 μg/mL) or isotype-treated (50 μg/mL) MIECs. Scale bar: 25 μm. (**E**) In vitro permeability assay of MIECs after VE-cadherin blockade with BV13 (normalized to untreated cells). Data are expressed as box-and-whisker plots. Horizontal bars indicate the median, box borders indicate the 25th and 75th percentiles, and whiskers indicate minimum and maximum values. (**A**–**D**) Nuclei stained by DRAQ5 (blue). Arrows indicate linear VE-cadherin and/or ZO-1 pattern at cell-cell contacts; asterisks display internalization. (**A**–**E**) One representative experiment of 3 independent experiments is depicted. One-way ANOVA with Tukey's post hoc test (**E**) was used (**$P < 0.01$).

that the regulation of angiogenesis is not the responsible pathogenic function of vessel-directed IFN-γ activity in IBD. This is supported by another study that showed that inhibition of angiogenesis by PGF knockout failed to ameliorate DSS-induced colitis (15), thus diminishing the role of angiogenesis in colitis promotion.

Interestingly, both anti–VEGF-A–treated control mice and Ifngr2$^{\Delta EC}$ mice with DSS-induced colitis exhibited significantly reduced vessel permeability, indicating that the impact of IFN-γ on the vascular barrier might be the driving force of its pathogenic effect. This is supported by our previous finding that overall blockade of IFN-γ in DSS-colitis inhibited vessel permeability (25), as well as by studies that have revealed an inducing effect of IFN-γ on endothelial cell permeability in vitro (22, 26). The clinical relevance of our hypothesis was supported by pCLE, showing that human IBD patients with active disease exhibit an increased vascular permeability compared with patients in remission or without IBD. Two studies further support our findings, as they showed increased vessel permeability in the colonic mucosa of IBD patients (16, 17). However, these studies did not analyze vessel permeability in relation to disease severity.

Multiple mechanisms have to be considered that might regulate IFN-γ–induced vessel permeability. Vascular permeability is dependent on (a) organ-specific functions of endothelial cells, including the lack or presence of fenestrations, which is not rele-

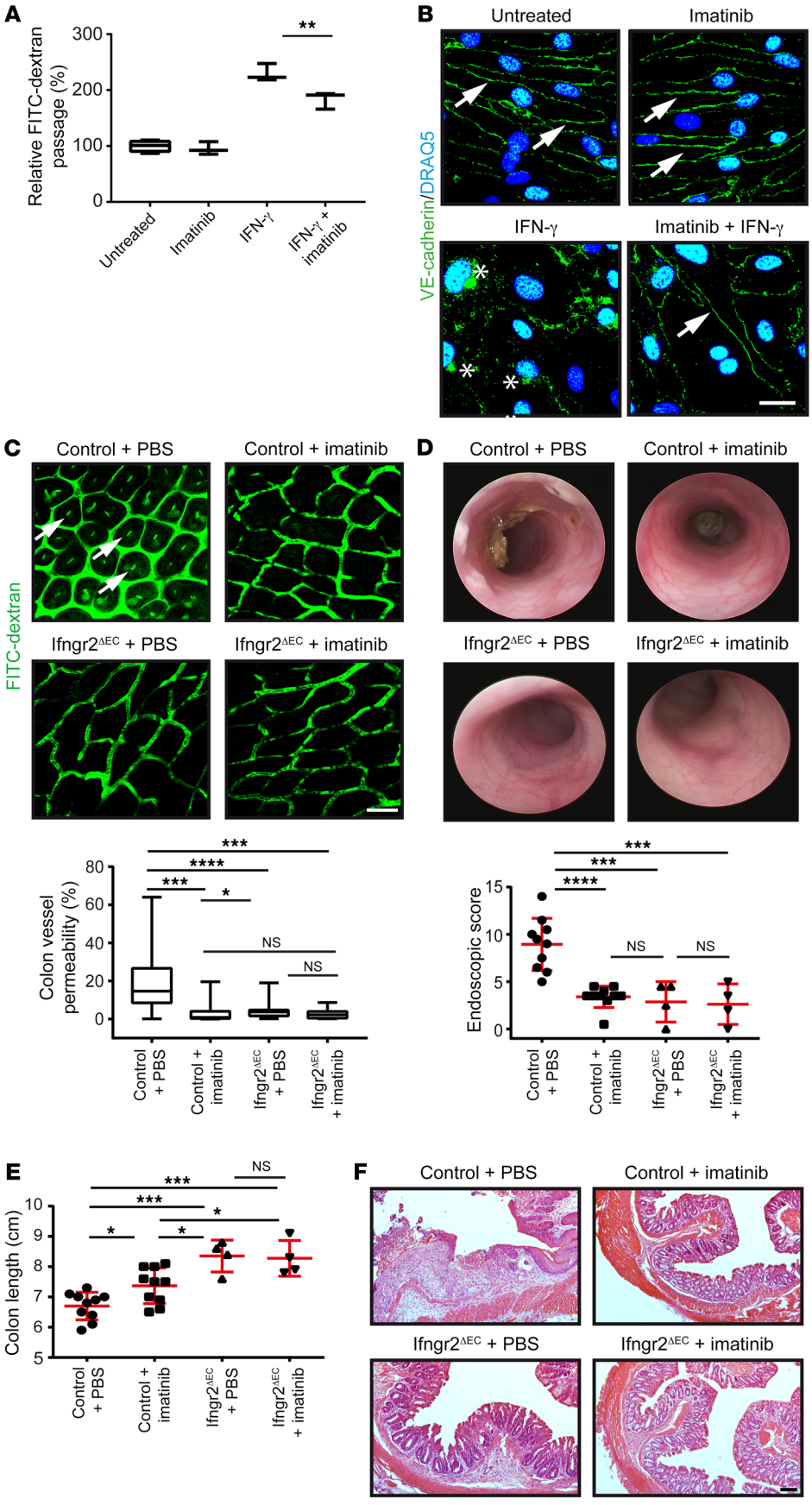

Figure 8. Treatment with imatinib restores vascular barrier function and reduces DSS-induced inflammation. (**A**) Imatinib (0.01 μg/mL) reduced IFN-γ–induced (100 U/mL) endothelial cell (MIEC) permeability in vitro; values are normalized to untreated cells. (**B**) Immunofluorescence staining of VE-cadherin (green), counterstained by DRAQ5 (blue), in MIECs treated with IFN-γ (100 U/mL), imatinib (0.01 μg/mL) plus IFN-γ, or imatinib alone or left untreated. Arrows indicate linear VE-cadherin pattern at cell-cell contacts; asterisks mark internalization. Scale bar: 25 μm. (**C**–**F**) Control mice received imatinib (n = 11) orally daily during the course of DSS-colitis or PBS only (n = 10) and were compared with Ifngr2$^{\Delta EC}$ mice receiving the same treatment (n = 3, imatinib; n = 4, PBS). (**C**) In vivo permeability of colonic vessels was assessed by i.v. injection of 70-kDa FITC-dextran (10 mg/mL). Accumulation in intestinal crypts (arrows) indicates vessel permeability, calculated as the ratio of FITC signal inside the crypts over the total FITC signal in percent (10 crypts per mouse). Scale bar: 50 μm. Treatment with imatinib reduced the severity of DSS-colitis in control mice evaluated by endoscopy (**D**), colon length (**E**), and histologic examination by H&E staining (**F**; scale bar: 100 μm). (**A** and **B**) One representative of 3 independent experiments is depicted. Quantitative evaluations are shown as box-and-whisker plots (**A** and **C**) (horizontal bars, median; box borders, 25th and 75th percentiles; whiskers, minimum and maximum values) or means ± SD (**D** and **E**). All graphs are means ± SD. One-way ANOVA followed by Tukey's post hoc test (**A**, **D**, and **E**) and Kruskal-Wallis test followed by Dunn's post hoc test (**C**) were used for statistical evaluation (*P < 0.05, **P < 0.01, ***P < 0.001, ****P < 0.0001). For genotypes of respective mice, see Supplemental Figure 1E.

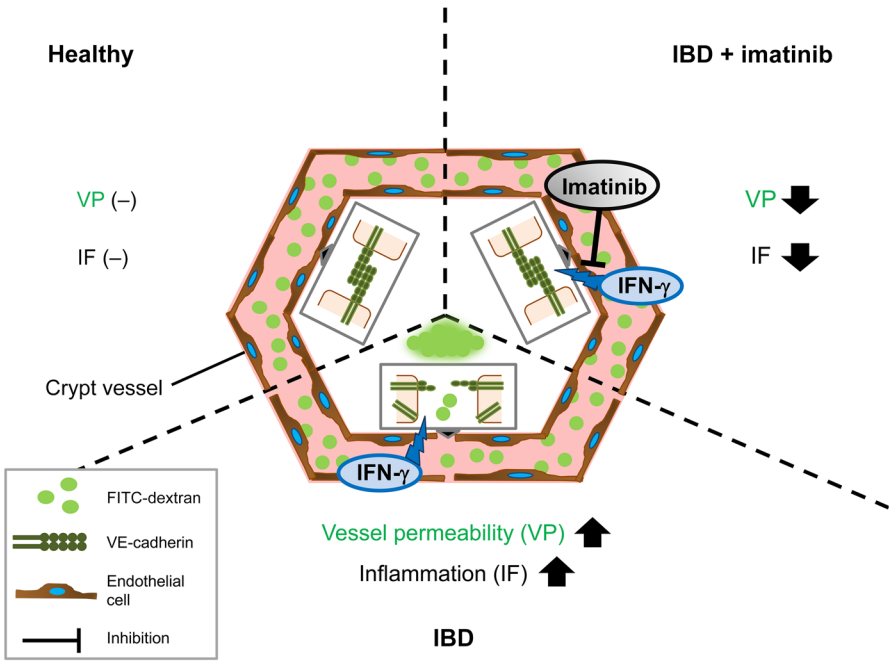

Figure 9. IFN-γ–induced vessel permeability and its inhibition by imatinib in IBD. IFN-γ increases permeability of intestinal vessels by disruption of VE-cadherin junctions, associated with increased inflammation and progression of IBD. Imatinib inhibits VE-cadherin disruption, reduces vascular permeability, and ameliorates the course of the disease. (–), normal level; black arrows, increase or decrease as compared with normal level.

vant to our study focusing on intestinal vessels (56, 57); (b) vessel maturation and concomitant coverage with mural cells (44, 46, 58); and (c) endothelial cell-cell interactions (45, 59). Interestingly, mural cell coverage of colon vessels was significantly increased in the DSS-induced colitis model when the vasculature could not respond to IFN-γ. Thus, reduced vessel maturation in the presence of IFN-γ might contribute to increased vessel permeability in IBD. Notably, vessel maturation is critically dependent on and might change with integrity variations of the endothelial layer. Accordingly, the molecular regulation of endothelial cell-cell contacts might represent the causative mechanism of the IFN-γ–induced vascular permeability increase.

Tight and adherens junctions are the 2 major components of the apical junction complex of endothelial cells (8, 60). In intestinal endothelial cells, tight junctions are composed of occludin, JAM-A, cingulin, and ZO-1, whereas adherens junctions are formed by VE-cadherin and β-catenin (6, 60). ZO-1 was not altered in the presence of IFN-γ, indicating that adherens junctions with VE-cadherin may be the major determinant of endothelial cell barrier function in our context. In fact, IFN-γ induced VE-cadherin disruption in cell culture, in agreement with 2 other studies (61, 62). VE-cadherin junctions were also disrupted in the intestinal vasculature in DSS-induced colitis. Notably, functional deactivation of VE-cadherin with a specific antibody (mAbBV13) was sufficient to significantly increase the permeability in confluent monolayers of MIECs, in accordance with the observations of Corada et al. (47). Most importantly, analyses of inflamed tissue areas of IBD patients showed that IFN-γ–induced disturbance of VE-cadherin also occurs in the course of the disease in humans. Altogether these findings support the conclusion that IBD-associated vascular barrier defects are predominantly due to IFN-γ–induced deactivation of VE-cadherin in adherens junctions.

VE-cadherin deactivation can occur by internalization (48) or by cleavage, leading to increased vessel permeability (49). For example, VE-cadherin was found to be degraded after treatment of endothelial cells with inflammatory stimuli, such as LPS and TNF-α (63, 64). In our study, we observed both internalization and proteolytic cleavage of VE-cadherin in the presence of IFN-γ. More precisely, an intracellular 35-kDa fragment of VE-cadherin, corresponding to the cytoplasmic domain of the molecule, was obtained in membrane fractions of MIECs after IFN-γ treatment (Supplemental Figure 10). Also, it has been previously shown that IFN-γ induces remodeling of the actin cytoskeleton in endothelial cells via GBP-1 (65), which might further amplify junctional VE-cadherin rearrangement in endothelial cells.

In the colon tissues of DSS-treated mice, increased vessel permeability correlated with the increased influx of immune cells, which might account for disease progression. In other studies, VE-cadherin–mediated regulation of vessel permeability has been associated with increased leukocyte extravasation (66, 67). A disrupted vascular barrier in the intestine might exert systemic effects in disease progression by fostering the translocation of intestinal bacteria into the blood and spreading to extraintestinal organs. A respective mechanism was observed in mice infected with *Salmonella*, which caused increased vessel permeability and subsequent dissemination of *Salmonella* to the liver and spleen (6). It is supposed that bacteremia in IBD patients leads to systemic inflammation and aberrant immune cell homing, which increases the risk of endocarditis and other extraintestinal manifestations, driving the morbidity associated with IBD (68, 69).

Traditional IBD medication aims to control the immune response with corticosteroids, aminosalicylates, and immunosuppressants (54). As these drugs show limited efficacy, variable responses, and strong side effects, efforts have been made in recent years to develop novel therapy options (1). The identification of IFN-γ–induced vascular barrier dysfunction as a driver of IBD pathogenesis opens new perspectives for the treatment of this disease.

Imatinib is a receptor tyrosine kinase inhibitor approved for cancer therapy (50). It was chosen as a candidate for vessel-directed IBD treatment in our studies, as it has been previously shown to also exert potent vascular effects. These include stabilizing the endothelial barrier by restoring VE-cadherin junctions in vitro and in mouse models of vascular leakage in skin, lung, and the blood-brain barrier and during sepsis (51–53). Most importantly, imatinib therapy of leukemia patients who sporadically suffered from UC and CD was associated with long-standing remission of UC/CD (70, 71).

Several putative mechanisms have been suggested to explain the clinical response to imatinib, such as its ability to inhibit macrophage activation and TNF-α production, mast cell c-kit signaling, and fibroblast PDGFR signaling and proliferation; to induce T cell apoptosis; or to target an unknown UC/CD-associated tyrosine kinase (70–72). Our findings suggest that the stabilization of VE-cadherin may be of major relevance. This correlated with a decreased permeability of IFN-γ–treated endothelial cells in vitro and an inhibition of DSS-colitis–induced vessel permeability in vivo, associated with a significantly improved disease course. All of these findings are well in agreement with a barrier-restoring function of imatinib and support the pathologic function of IFN-γ–induced vascular permeability in IBD.

Recently it has been shown that IFN-γ can induce members of the Abelson (Abl) family of nonreceptor tyrosine kinases in certain cell types (73). Notably, Abl kinases are required for VEGF- and thrombin-induced disruption of adherens junctions, and imatinib is a potent inhibitor of Abl kinase activity (74, 75). Accordingly, it may be promising in future studies to investigate whether imatinib stabilizes VE-cadherin at endothelial adherens junctions in IBD through inhibition of Abl kinase activity.

The clinical responses of UC/CD patients under imatinib treatment might be due to the restoration of the endothelial barrier, which opens attractive future perspectives. First, pCLE-based determination of vessel permeability (Figure 5E) could be applied to monitor vascular-directed effects of presently used IBD therapy. For example, fontolizumab, an IFN-γ inhibitor, has yielded only limited therapeutic responses in IBD patients (76–78). However, fontolizumab therapy was not controlled for its impact on vascular permeability, which might improve the identification of effective treatment doses and patients responding to this therapy. Second, the inflamed intestinal vasculature might provide a novel therapeutic target in the treatment of IBD. In this framework, our results identify imatinib as a prime candidate for clinical pilot studies.

Methods

Patients

Intestinal tissues from inflamed and uninvolved areas of the same patients suffering from CD and UC were obtained by surgery. Tissue samples were formalin-fixed and paraffin-embedded. After H&E staining, the degree of inflammation and mucosal damage was determined by a pathologist in a blinded fashion (Supplemental Table 2).

Patients included in the study with probe-based confocal laser endomicroscopy (pCLE) had endoscopically and histologically confirmed UC. Active disease was defined via clinical scoring systems (e.g., the Mayo Clinical Score) (79, 80) (Supplemental Table 1). As healthy controls, patients without inflammation admitted for pCLE for other diagnostic reasons were included. See also "Study approval" below.

Transgenic mice

C57BL/6J endothelial cell–specific *Ifngr2*-knockout mice (referred to as Ifngr2$^{\Delta EC}$) were generated by crossing of *C57BL/6J Ifngr2$^{fl/fl}$* mice (previously described, refs. 81, 82) with *B6.Cg-Tg(Tek-cre)12Flv/J* mice (also known as *Tie-2-Cre*; previously described, ref. 33). Tamoxifen-inducible endothelial cell–specific *Ifngr2*-knockout mice (Ifngr2$^{i\Delta EC}$) were obtained by crossing of *Ifngr2$^{fl/fl}$* mice with *Cdh5-CreERT2* mice (34). Postnatal *Ifngr2* deletion was induced by administration of 4-hydroxytamoxifen (150 μg per 30 g of body weight; Cayman Chemical Co.) through i.p. injection into 4- to 5-week-old mice. Injections were performed once per day for 5 consecutive days. Sex- and age-matched, cohoused littermates at weeks 6–12 of age were used for each experiment. *C57BL/6J Ifngr2$^{fl/fl}$* mice were used as control. Both female and male mice were used. All mice were housed in specific pathogen–free conditions and were routinely screened for pathogens according to Federation of European Laboratory Animal Science Associations (FELASA) guidelines. All mice had ad libitum access to a standard diet and water.

Bone marrow transplantation of mice

As *Tie2* is expressed not only by vascular endothelial cells but also by hematopoietic cells (35), both Ifngr2$^{\Delta EC}$ and control mice underwent bone marrow transplantation with wild-type bone marrow cells to guarantee that IFN-γ receptor 2 was only deleted in endothelial cells. Recipient mice (CD45.2) were irradiated with 9 Gy (BioBeam, GammaService Medical GmbH). The next day, i.v. reconstitution with 0.7×10^6 bone marrow cells per mouse in PBS isolated from femurs of CD45.1 donor mice (B6 Cd45.1, Pep Boy, The Jackson Laboratory) was performed. Antibiotics (2.5% Baytril, Bayer) were applied in the drinking water for 10 days. The blood of recipients was analyzed after 6 weeks of reconstitution by flow cytometry (Supplemental Methods).

Induction, treatment, and evaluation of DSS-induced colitis

To induce acute DSS-colitis in Ifngr2$^{\Delta EC}$ mice, 2.5% DSS (40 kDa; MP Biomedicals) was added to the drinking water for a 7-day cycle, and subsequently, normal drinking water was given for 3 days. For induction of chronic colitis, DSS was applied in 3 consecutive cycles with 2-week intervals. In Ifngr2$^{i\Delta EC}$ mice, acute DSS-colitis was induced between 10 and 25 days after the last tamoxifen injection. On day 9 of the last cycle of DSS treatment, mice were anesthetized with isoflurane (2%, 2 L/min; CP-Pharma), and the intestinal mucosa was analyzed by high-resolution mini-endoscopy (Karl-Storz) to determine the grade of colitis. A disease-specific scoring system adapted from Becker et al. (37) was used to grade intestinal inflammation, which considered thickening of the colon wall, changes in the normal vascular pattern, presence of fibrin, mucosal granularity, and stool consistency with numerical scores between 0 and 3 each, with 15 being the maximal score at conditions of most severe colitis. After day 10, mice were sacrificed by cervical dislocation, and the colon tissue was removed from the cecum to the rectum. Colon length was measured, and subsequently, the tissues were processed for histologic analyses. The same area of the distal colon was analyzed for all described experiments.

VEGF blockade. Endogenous VEGF-A activity was blocked by administration of anti–VEGF-A antibody (150 μg/mouse in PBS; B20-

4.1.1, Genentech Inc.; refs. 41, 42) by i.p. injection daily within the first 5 days of DSS-colitis, followed by injection every 2 days until the final day of the experiment. As a control, a mouse IgG2a isotype control antibody (150 μg/mouse in PBS; clone MOPC-173, catalog 400281, BioLegend) was applied.

Imatinib administration. Starting from the first day of DSS, imatinib (Gleevec, Novartis) was given orally by a feeding needle (Fine Science Tools) once a day within the first 6 days at a concentration of 50 mg/kg dissolved in PBS. Subsequently, the dosage was increased to 100 mg/kg twice per day until the final day of DSS-colitis. The application of PBS served as a control.

Metatarsal assay

Metatarsal bones were isolated from embryos of day 18.5, cultured, and stained as previously described (40). Sprouting capillaries were stained with a rat anti–mouse CD31 antibody (1:400; catalog DIA310, Dianova) and an AF488-conjugated donkey anti-rat secondary antibody (1:500; catalog A-21208, Thermo Fisher Scientific). A laser-scanning confocal microscope (TCS SPE, Leica Microsystems; equipped with LAS-LAF software) was used to visualize metatarsals via tile scans.

Immunohistochemistry of human and murine colonic tissues

Immunohistochemistry of human and mouse colon tissues was carried out as described previously (27, 31). Antigen retrieval was performed in target retrieval solution, pH 9.0 (TRS9, Dako). The following primary antibodies were used for 1 hour at room temperature: rat anti–mouse CD31 (1:100; catalog DIA310, Dianova), rabbit anti–mouse Ifngr2 (1:500; generated by immunization with the peptide HYWEKSETQQEQVEGPFKS corresponding to amino acids 171–189 in the C-terminal extracellular domain of Ifngr2; Pineda Antikörper Service), rat anti–mouse CD45 (1:500; catalog 103102, BioLegend), rabbit anti–mouse CD4 (1:500; catalog ab183685, Abcam), rat anti–mouse F4/80 (1:250; catalog 14-4801-81, eBioscience), rabbit anti–mouse Ki-67 (1:50; catalog ab16667, Abcam), rabbit anti–mouse α-SMA (1:1000; catalog ab124964, Abcam), rabbit anti–human PDGFR-β (1:100; catalog ab32570, Abcam), mouse anti–human CD31 (20.5 μg/mL; clone JC70A, catalog M0823, Dako), and rabbit anti–human VE-cadherin (1:100; catalog ab33168, Abcam). As isotype controls, the following antibodies in the same final concentrations as the respective detection antibodies were used: mouse IgG1 (catalog MAB002), rat IgG2b (catalog MAB0061), rat IgG2a (catalog MAB006), and rabbit IgG (catalog AB-105-C), all from R&D Systems. As secondary antibodies, AF488-conjugated donkey anti-rat (1:500; catalog A-21208), AF546-conjugated donkey anti-rabbit (1:500; catalog A10040), AF488-conjugated donkey anti-rabbit (1:500; catalog A-21206), AF488-conjugated goat anti-rat (1:500; catalog A-11006), AF546-conjugated goat anti-rabbit (1:500; catalog A-11035), and AF488-conjugated donkey anti-mouse (1:500; catalog A-21202), all from Thermo Fisher Scientific, were used for 45 minutes at room temperature. Nuclei were stained with DRAQ5 (1:800; catalog 4084, Cell Signaling Technology), and slides were mounted with fluorescence mounting medium (Dako). Stainings with respective isotype controls for each antibody are shown in Supplemental Figure 11. The immune cell infiltration (CD45, CD4, F4/80) was quantified by counting of the number of $CD45^+$, $CD4^+$, or $F4/80^+$ cells per field using ImageJ/Fiji (NIH) (83). The overall number of cells per field was counted based on nuclear staining. The number of immune cells was determined as the ratio of $CD45^+$, $CD4^+$, or $F4/80^+$ cells over the total cell number per field and was given as a percentage.

Cell culture

C57BL/6 mouse small intestinal endothelial cells (MIECs) were purchased from Cell Biologics, kept in complete mouse endothelial cell medium with the growth factor supplement (Cell Biologics), and routinely tested for mycoplasma negativity using the MycoAlert Mycoplasma Detection Kit (Lonza). As a starvation medium, basal mouse endothelial cell medium (Cell Biologics) with 0.5% FCS and without growth factor supplement was used. Cells in passages 4–6 were used for the experiments. HUVECs were purchased from Lonza and cultured in endothelial growth medium 2 (EGM-2, Lonza). Cells between passages 3 and 5 were used. Normal human lung fibroblasts (LFs) from Lonza were cultured in fibroblast growth medium 2 (FGM-2, Lonza) and used between passages 5 and 6. All cells were maintained in a humidified incubator at 37°C and 5% CO_2.

Supplemental Methods

Mouse genotyping; cell isolation from mouse spleen, blood, thymus, and lung; immune cell phenotyping by flow cytometry; isolation of RNA from mouse lung endothelial cells and bone marrow cells; quantitative reverse transcriptase PCR; Western blot of MIEC membrane fractions; immunocytochemistry; proliferation assay of MIECs; microfluidic 3D angiogenesis and vasculogenesis model; in vitro permeability assay; confocal laser endomicroscopy; intravital microscopy; 2-photon microscopy; and light-sheet microscopy were performed as indicated in Supplemental Methods online.

Statistics

Statistical analyses of pairwise comparisons were performed using 2-tailed, unpaired Student's *t* test for normally distributed data. For data without normal distribution, the Mann-Whitney *U* test was used. Multiple comparisons were analyzed via 1-way ANOVA followed by Tukey's multiple-comparisons post hoc test or via Kruskal-Wallis test followed by Dunn's multiple-comparisons post hoc test for non-normal distribution. For 2 different categorical variables, 2-way ANOVA followed by Šidák's multiple-comparisons post hoc test was used. To compare sampling distributions, the χ^2 test was used. For all analyses, GraphPad Prism software version 6.00 (GraphPad Software) was used. *P* values less than 0.05 were considered significant.

Study approval

Patients. All procedures were approved by the local ethics committee of the University of Erlangen-Nuremberg (no. 91_18 B, Ethikkomission der FAU, Erlangen, Germany). Patients gave written informed consent before participation in this study.

Animal experimentation. All animal studies were performed in accordance with German law and approved by the Institutional Animal Care and Use Committee of the University of Erlangen and the Animal Experiment Committee of the State Government of Lower Franconia, Würzburg, Germany (55.2-2532-2-366 and 55.2-2532.1-37/14).

Author contributions

VL, NBL, and M Stürzl designed the experiments. VL, DR, NBL, EN, VK, THW, LS, SL, EV, and KS performed the experiments. VL, NBL, BS, MJW, EN, PT, and M Stürzl analyzed the data. CIG ana-

lyzed pathologic specimens. CH, SK, and TR recruited patients and provided human specimens or human endoscopy data. THW, MJW, CB, BS, PT, NLJ, RHA, TW, AR, and M Schumann provided key reagents, materials, analysis tools, and/or helpful ideas. VL, NBL, and M Stürzl wrote the manuscript. All of the authors approved the final version of the manuscript.

Acknowledgments

We thank the Optical Imaging Centre Erlangen (Erlangen, Germany) for excellent support in microscopic techniques, Werner Muller (Division of Infection, Immunity & Respiratory Medicine, University of Manchester, Manchester, United Kingdom) for providing C57BL/6J *Ifngr2*$^{fl/fl}$ mice, and Reiner Strick (Clinics of Obstetrics and Gynaecology, Friedrich-Alexander University Erlangen-Nuremberg, Erlangen, Germany) for continuous mentoring. Special thanks to Regine Schneider-Stock (Institute of Pathology, Friedrich-Alexander University Erlanigen-Nuremberg, Erlangen, Germany), Clemens Neufert (Medical Clinic I, Friedrich-Alexander University Erlangen-Nuremberg, Erlangen, Germany), and the Rudolf-Bartling Stiftung, Hannover, Germany, for providing the mini-endoscope. This work was performed in (partial) fulfillment of the requirements for obtaining the degree Dr. rer. nat. by Victoria Langer. Supporting grants were from the German Research Foundation (DFG) (KFO 257 [subproject 4 to M Stürzl and MJW], FOR 2438 [subproject 2 to EN and M Stürzl], SFB/TRR241 [subproject A06 to M Stürzl and NBL], and BR 5196/2-1 [to NBL]); the Interdisciplinary Center for Clinical Research (IZKF) of the Clinical Center Erlangen (D28 to EN and M Stürzl); the W. Lutz Stiftung (to M Stürzl); and the Forschungsstiftung Medizin am Universitätsklinikum Erlangen (to M Stürzl).

Address correspondence to: Michael Stürzl, Division of Molecular and Experimental Surgery, Translational Research Center, Department of Surgery, University Medical Center Erlangen, Friedrich-Alexander University Erlangen-Nürnberg, Schwabachanlage 12, 91054 Erlangen, Germany. Phone: 49.9131.85.39522; Email: michael.stuerzl@uk-erlangen.de.

KS's present address is: Department of Dermatology and Allergy, Technical University of Munich, Munich, Germany.

LS's present address is: Cosphatec GmbH, Hamburg, Germany.

1. Rutgeerts P, Vermeire S, Van Assche G. Biological therapies for inflammatory bowel diseases. *Gastroenterology*. 2009;136(4):1182–1197.
2. Ng SC, et al. Worldwide incidence and prevalence of inflammatory bowel disease in the 21st century: a systematic review of population-based studies. *Lancet*. 2018;390(10114):2769–2778.
3. Uhlig HH, Powrie F. Dendritic cells and the intestinal bacterial flora: a role for localized mucosal immune responses. *J Clin Invest*. 2003;112(5):648–651.
4. Neurath MF. Cytokines in inflammatory bowel disease. *Nat Rev Immunol*. 2014;14(5):329–342.
5. Peterson LW, Artis D. Intestinal epithelial cells: regulators of barrier function and immune homeostasis. *Nat Rev Immunol*. 2014;14(3):141–153.
6. Spadoni I, et al. A gut-vascular barrier controls the systemic dissemination of bacteria. *Science*. 2015;350(6262):830–834.
7. Cromer WE, Mathis JM, Granger DN, Chaitanya GV, Alexander JS. Role of the endothelium in inflammatory bowel diseases. *World J Gastroenterol*. 2011;17(5):578–593.
8. Komarova YA, Kruse K, Mehta D, Malik AB. Protein interactions at endothelial junctions and signaling mechanisms regulating endothelial permeability. *Circ Res*. 2017;120(1):179–206.
9. Habtezion A, Nguyen LP, Hadeiba H, Butcher EC. Leukocyte trafficking to the small intestine and colon. *Gastroenterology*. 2016;150(2):340–354.
10. Danese S, et al. Angiogenesis as a novel component of inflammatory bowel disease pathogenesis. *Gastroenterology*. 2006;130(7):2060–2073.
11. Scaldaferri F, et al. VEGF-A links angiogenesis and inflammation in inflammatory bowel disease pathogenesis. *Gastroenterology*. 2009;136(2):585–595.e5.
12. Alkim C, Alkim H, Koksal AR, Boga S, Sen I. Angiogenesis in inflammatory bowel disease. *Int J Inflam*. 2015;2015:970890.
13. Cromer WE, et al. VEGF-A isoform modulation in an preclinical TNBS model of ulcerative colitis: protective effects of a VEGF164b therapy. *J Transl Med*. 2013;11:207.
14. Tolstanova G, et al. Neutralizing anti-vascular endothelial growth factor (VEGF) antibody reduces severity of experimental ulcerative colitis in rats: direct evidence for the pathogenic role of VEGF. *J Pharmacol Exp Ther*. 2009;328(3):749–757.
15. Hindryckx P, et al. Absence of placental growth factor blocks dextran sodium sulfate-induced colonic mucosal angiogenesis, increases mucosal hypoxia and aggravates acute colonic injury. *Lab Invest*. 2010;90(4):566–576.
16. Buda A, et al. Confocal laser endomicroscopy for prediction of disease relapse in ulcerative colitis: a pilot study. *J Crohns Colitis*. 2014;8(4):304–311.
17. Macé V, et al. Confocal laser endomicroscopy: a new gold standard for the assessment of mucosal healing in ulcerative colitis. *J Gastroenterol Hepatol*. 2015;30(suppl 1):85–92.
18. Verma R, Verma N, Paul J. Expression of inflammatory genes in the colon of ulcerative colitis patients varies with activity both at the mRNA and protein level. *Eur Cytokine Netw*. 2013;24(3):130–138.
19. Ito R, et al. Interferon-gamma is causatively involved in experimental inflammatory bowel disease in mice. *Clin Exp Immunol*. 2006;146(2):330–338.
20. Singh UP, et al. Chemokine and cytokine levels in inflammatory bowel disease patients. *Cytokine*. 2016;77:44–49.
21. Rafa H, et al. Involvement of interferon-γ in bowel disease pathogenesis by nitric oxide pathway: a study in Algerian patients. *J Interferon Cytokine Res*. 2010;30(9):691–697.
22. Oshima T, et al. Interferon-gamma and interleukin-10 reciprocally regulate endothelial junction integrity and barrier function. *Microvasc Res*. 2001;61(1):130–143.
23. Lee HN, et al. Dendritic cells expressing immunoreceptor CD300f are critical for controlling chronic gut inflammation. *J Clin Invest*. 2017;127(5):1905–1917.
24. Nava P, et al. Interferon-gamma regulates intestinal epithelial homeostasis through converging beta-catenin signaling pathways. *Immunity*. 2010;32(3):392–402.
25. Haep L, et al. Interferon gamma counteracts the angiogenic switch and induces vascular permeability in dextran sulfate sodium colitis in mice. *Inflamm Bowel Dis*. 2015;21(10):2360–2371.
26. Ng CT, Fong LY, Low YY, Ban J, Hakim MN, Ahmad Z. Nitric oxide participates in IFN-γ-induced HUVECs hyperpermeability. *Physiol Res*. 2016;65(6):1053–1058.
27. Naschberger E, et al. Matricellular protein SPARCL1 regulates tumor microenvironment-dependent endothelial cell heterogeneity in colorectal carcinoma. *J Clin Invest*. 2016;126(11):4187–4204.
28. Weinländer K, et al. Guanylate binding protein-1 inhibits spreading and migration of endothelial cells through induction of integrin alpha4 expression. *FASEB J*. 2008;22(12):4168–4178.
29. Guenzi E, et al. The guanylate binding protein-1 GTPase controls the invasive and angiogenic capability of endothelial cells through inhibition of MMP-1 expression. *EMBO J*. 2003;22(15):3772–3782.
30. Guenzi E, et al. The helical domain of GBP-1 mediates the inhibition of endothelial cell proliferation by inflammatory cytokines. *EMBO J*. 2001;20(20):5568–5577.
31. Naschberger E, et al. Angiostatic immune reaction in colorectal carcinoma: impact on survival and perspectives for antiangiogenic therapy. *Int J Cancer*. 2008;123(9):2120–2129.
32. Schroder K, Hertzog PJ, Ravasi T, Hume DA. Interferon-gamma: an overview of signals, mechanisms and functions. *J Leukoc Biol*. 2004;75(2):163–189.

33. Schlaeger TM, et al. Uniform vascular-endothelial-cell-specific gene expression in both embryonic and adult transgenic mice. *Proc Natl Acad Sci U S A*. 1997;94(7):3058–3063.
34. Sörensen I, Adams RH, Gossler A. DLL1-mediated Notch activation regulates endothelial identity in mouse fetal arteries. *Blood*. 2009;113(22):5680–5688.
35. Tang Y, Harrington A, Yang X, Friesel RE, Liaw L. The contribution of the Tie^{2+} lineage to primitive and definitive hematopoietic cells. *Genesis*. 2010;48(9):563–567.
36. Payne S, De Val S, Neal A. Endothelial-specific Cre mouse models. *Arterioscler Thromb Vasc Biol*. 2018;38(11):2550–2561.
37. Becker C, Fantini MC, Neurath MF. High resolution colonoscopy in live mice. *Nat Protoc*. 2006;1(6):2900–2904.
38. Kim S, Chung M, Ahn J, Lee S, Jeon NL. Interstitial flow regulates the angiogenic response and phenotype of endothelial cells in a 3D culture model. *Lab Chip*. 2016;16(21):4189–4199.
39. Kim S, Lee H, Chung M, Jeon NL. Engineering of functional, perfusable 3D microvascular networks on a chip. *Lab Chip*. 2013;13(8):1489–1500.
40. Song W, et al. The fetal mouse metatarsal bone explant as a model of angiogenesis. *Nat Protoc*. 2015;10(10):1459–1473.
41. Liang WC, et al. Cross-species vascular endothelial growth factor (VEGF)-blocking antibodies completely inhibit the growth of human tumor xenografts and measure the contribution of stromal VEGF. *J Biol Chem*. 2006;281(2):951–961.
42. Fuh G, et al. Structure-function studies of two synthetic anti-vascular endothelial growth factor Fabs and comparison with the Avastin Fab. *J Biol Chem*. 2006;281(10):6625–6631.
43. Aragon-Sanabria V, Pohler SE, Eswar VJ, Bierowski M, Gomez EW, Dong C. VE-cadherin disassembly and cell contractility in the endothelium are necessary for barrier disruption induced by tumor cells. *Sci Rep*. 2017;7:45835.
44. Bergers G, Song S. The role of pericytes in blood-vessel formation and maintenance. *Neuro-oncology*. 2005;7(4):452–464.
45. Vickerman V, Kamm RD. Mechanism of a flow-gated angiogenesis switch: early signaling events at cell-matrix and cell-cell junctions. *Integr Biol (Camb)*. 2012;4(8):863–874.
46. Jain RK. Molecular regulation of vessel maturation. *Nat Med*. 2003;9(6):685–693.
47. Corada M, et al. Vascular endothelial-cadherin is an important determinant of microvascular integrity in vivo. *Proc Natl Acad Sci U S A*. 1999;96(17):9815–9820.
48. Gavard J, Gutkind JS. VEGF controls endothelial-cell permeability by promoting the beta-arrestin-dependent endocytosis of VE-cadherin. *Nat Cell Biol*. 2006;8(11):1223–1234.
49. Dejana E, Orsenigo F, Lampugnani MG. The role of adherens junctions and VE-cadherin in the control of vascular permeability. *J Cell Sci*. 2008;121(pt 13):2115–2122.
50. Iqbal N, Iqbal N. Imatinib: a breakthrough of targeted therapy in cancer. *Chemother Res Pract*. 2014;2014:357027.
51. Aman J, et al. Effective treatment of edema and endothelial barrier dysfunction with imatinib. *Circulation*. 2012;126(23):2728–2738.
52. Armulik A, et al. Pericytes regulate the blood-brain barrier. *Nature*. 2010;468(7323):557–561.
53. Letsiou E, et al. Differential and opposing effects of imatinib on LPS- and ventilator-induced lung injury. *Am J Physiol Lung Cell Mol Physiol*. 2015;308(3):L259–L269.
54. Podolsky DK. Inflammatory bowel disease. *N Engl J Med*. 2002;347(6):417–429.
55. Jostins L, et al. Host-microbe interactions have shaped the genetic architecture of inflammatory bowel disease. *Nature*. 2012;491(7422):119–124.
56. Rafii S, Butler JM, Ding BS. Angiocrine functions of organ-specific endothelial cells. *Nature*. 2016;529(7586):316–325.
57. Stan RV, et al. The diaphragms of fenestrated endothelia: gatekeepers of vascular permeability and blood composition. *Dev Cell*. 2012;23(6):1203–1218.
58. Armulik A, Genové G, Betsholtz C. Pericytes: developmental, physiological, and pathological perspectives, problems, and promises. *Dev Cell*. 2011;21(2):193–215.
59. Cerutti C, Ridley AJ. Endothelial cell-cell adhesion and signaling. *Exp Cell Res*. 2017;358(1):31–38.
60. López-Posadas R, Stürzl M, Atreya I, Neurath MF, Britzen-Laurent N. Interplay of GTPases and cytoskeleton in cellular barrier defects during gut inflammation. *Front Immunol*. 2017;8:1240.
61. Herwig MC, Tsokos M, Hermanns MI, Kirkpatrick CJ, Müller AM. Vascular endothelial cadherin expression in lung specimens of patients with sepsis-induced acute respiratory distress syndrome and endothelial cell cultures. *Pathobiology*. 2013;80(5):245–251.
62. Chrobak I, Lenna S, Stawski L, Trojanowska M. Interferon-γ promotes vascular remodeling in human microvascular endothelial cells by upregulating endothelin (ET)-1 and transforming growth factor (TGF) β2. *J Cell Physiol*. 2013;228(8):1774–1783.
63. Flemming S, et al. Soluble VE-cadherin is involved in endothelial barrier breakdown in systemic inflammation and sepsis. *Cardiovasc Res*. 2015;107(1):32–44.
64. Sidibé A, et al. Soluble VE-cadherin in rheumatoid arthritis patients correlates with disease activity: evidence for tumor necrosis factor α-induced VE-cadherin cleavage. *Arthritis Rheum*. 2012;64(1):77–87.
65. Ostler N, et al. Gamma interferon-induced guanylate binding protein 1 is a novel actin cytoskeleton remodeling factor. *Mol Cell Biol*. 2014;34(2):196–209.
66. Schulte D, et al. Stabilizing the VE-cadherin-catenin complex blocks leukocyte extravasation and vascular permeability. *EMBO J*. 2011;30(20):4157–4170.
67. Wessel F, et al. Leukocyte extravasation and vascular permeability are each controlled in vivo by different tyrosine residues of VE-cadherin. *Nat Immunol*. 2014;15(3):223–230.
68. Kreuzpaintner G, Horstkotte D, Heyll A, Lösse B, Strohmeyer G. Increased risk of bacterial endocarditis in inflammatory bowel disease. *Am J Med*. 1992;92(4):391–395.
69. Mateer SW, et al. IL-6 drives neutrophil-mediated pulmonary inflammation associated with bacteremia in murine models of colitis. *Am J Pathol*. 2018;188(7):1625–1639.
70. Magro F, Costa C. Long-standing remission of Crohn's disease under imatinib therapy in a patient with Crohn's disease. *Inflamm Bowel Dis*. 2006;12(11):1087–1089.
71. Awano N, Ryu T, Yoshimura N, Takazoe M, Kitamura S, Tanaka M. Successful treatment of ulcerative colitis associated with hypereosinophilic syndrome/chronic eosinophilic leukemia. *Intern Med*. 2011;50(16):1741–1745.
72. De Backer O, Lefebvre RA. Is there a role for imatinib in inflammatory bowel disease? *Inflamm Bowel Dis*. 2008;14(4):579–581.
73. Ren WB, et al. Interferon-γ regulates cell malignant growth via the c-Abl/HDAC2 signaling pathway in mammary epithelial cells. *J Zhejiang Univ Sci B*. 2019;20(1):39–48.
74. Rizzo AN, Aman J, van Nieuw Amerongen GP, Dudek SM. Targeting Abl kinases to regulate vascular leak during sepsis and acute respiratory distress syndrome. *Arterioscler Thromb Vasc Biol*. 2015;35(5):1071–1079.
75. Chislock EM, Pendergast AM. Abl family kinases regulate endothelial barrier function in vitro and in mice. *PLoS One*. 2013;8(12):e85231.
76. Hommes DW, et al. Fontolizumab, a humanised anti-interferon gamma antibody, demonstrates safety and clinical activity in patients with moderate to severe Crohn's disease. *Gut*. 2006;55(8):1131–1137.
77. Reinisch W, et al. Fontolizumab in moderate to severe Crohn's disease: a phase 2, randomized, double-blind, placebo-controlled, multiple-dose study. *Inflamm Bowel Dis*. 2010;16(2):233–242.
78. Reinisch W, et al. A dose escalating, placebo controlled, double blind, single dose and multidose, safety and tolerability study of fontolizumab, a humanised anti-interferon gamma antibody, in patients with moderate to severe Crohn's disease. *Gut*. 2006;55(8):1138–1144.
79. D'Haens G, et al. A review of activity indices and efficacy end points for clinical trials of medical therapy in adults with ulcerative colitis. *Gastroenterology*. 2007;132(2):763–786.
80. Schroeder KW, Tremaine WJ, Ilstrup DM. Coated oral 5-aminosalicylic acid therapy for mildly to moderately active ulcerative colitis. A randomized study. *N Engl J Med*. 1987;317(26):1625–1629.
81. Lee HM, et al. IFNγ signaling endows DCs with the capacity to control type I inflammation during parasitic infection through promoting $T\text{-}bet^{+}$ regulatory T cells. *PLoS Pathog*. 2015;11(2):e1004635.
82. Villegas-Mendez A, et al. Gamma interferon mediates experimental cerebral malaria by signaling within both the hematopoietic and nonhematopoietic compartments. *Infect Immun*. 2017;85(11):e01035-16.
83. Schindelin J, et al. Fiji: an open-source platform for biological-image analysis. *Nat Methods*. 2012;9(7):676–682.